Article

SOURCE DATA | TRANSPARENT PROCESS | OPEN ACCESS

EMBO reports

Tonic TNF conditioning of macrophages safeguards stimulus-specific inflammatory responses

Stefanie Luecke[1,†], Adewunmi Adelaja[1,†,‡], Xiaolu Guo[1], Supriya Sen[1,§], Roberto Spreafico[1], Apeksha Singh[1], Yi Liu[1,¶], Brooks Taylor[1], Jessica Diaz[1], Quen Cheng[2] & Alexander Hoffmann[1,*]

Abstract

Tumor necrosis factor (TNF) is a key inflammatory cytokine that warns recipient cells of a nearby infection or tissue damage. Acute exposure to TNF activates characteristic oscillatory dynamics of the transcription factor NFκB and induces a characteristic gene expression program; these are distinct from the responses of cells directly exposed to pathogen-associated molecular patterns (PAMPs). Here, we report that tonic TNF exposure is critical for safeguarding TNF's specific functions. In the absence of tonic TNF conditioning, acute exposure to TNF causes (i) NFκB signaling dynamics that are less oscillatory and more like PAMP-responsive NFκB dynamics, (ii) immune gene expression that is more similar to the Pam3CSK4 response program, and (iii) broader epigenomic reprogramming that is characteristic of PAMP-responsive changes. We show that the absence of tonic TNF signaling effects subtle changes to TNF receptor availability and dynamics such that enhanced pathway activity results in non-oscillatory NFκB. Our results reveal tonic TNF as a key tissue determinant of the specific cellular responses to acute paracrine TNF exposure, and their distinction from responses to direct exposure to PAMPs.

Keywords epigenome integrity; immune sentinel cells; inflammation; NFκB dynamics; tonic TNF

Subject Categories Chromatin, Transcription, & Genomics; Immunology; Signal Transduction

DOI 10.15252/embr.202255986 | Received 18 August 2022 | Revised 2 May 2023 | Accepted 9 May 2023

EMBO Reports (2023) e55986

Introduction

Tumor necrosis factor (TNF) is a prominent inflammatory cytokine that elicits cellular responses to infection and injury. Dysregulation of TNF expression or TNF receptor signaling can contribute to inflammatory pathologies (Kalliolias & Ivashkiv, 2016). Indeed, TNF inhibition is common therapeutic approach for auto-inflammatory diseases such as rheumatoid arthritis and inflammatory bowel disease (Toussirot & Aubin, 2016). TNF is expressed and secreted by immune sentinel cells such as macrophages and fibroblasts and by immune effector cells such as NK cells and T cells (Sedger & McDermott, 2014). Its expression and secretion are induced by exposure to pathogen-associated molecular patterns (PAMPs) and warn bystander cells of danger. Almost all cell types respond to TNF via one or two receptors, TNFR1 and TNFR2. Upon TNF binding, TNFR is internalized via clathrin-mediated endocytosis. Cell surface signaling favors NFκB and MAPK activation via ubiquitin-mediated activation of IKK and TAK1, while endosomal signaling may trigger cell death (Schütze *et al*, 2008; Kalliolias & Ivashkiv, 2016).

The transcription factor NFκB, a major regulator of inflammatory gene expression, is activated by exposure to not only TNF but also PAMPs. Its activity shows intricate temporal patterns, which are dependent on the activating stimulus (Hoffmann *et al*, 2002; Covert *et al*, 2005; Werner *et al*, 2005; Adelaja *et al*, 2021). In response to TNF, NFκB dynamics show characteristic oscillations, while the TLR2/1-binding MyD88-dependent PAMP Pam3CSK4 (P3C4) elicits sustained, non-oscillatory responses (Adelaja *et al*, 2021). The oscillatory content of NFκB dynamics is determined by the level of IKK activity and the NFκB-responsive IκBα-negative feedback loop: sustained intermediate IKK activity allows for oscillations, while high activity neutralizes the feedback loop and results in non-oscillatory dynamics (Adelaja *et al*, 2021). The stimulus information contained in NFκB dynamics is decoded in the nucleus. Target genes are capable of distinguishing among peak activation fold (Lee *et al*, 2014), duration (Hoffmann *et al*, 2002; Sen *et al*, 2020), and speed (Ando *et al*, 2021). Interestingly, oscillatory dynamics (elicited by TNF) safeguard the epigenome, whereas non-oscillatory dynamics (elicited by PAMPs) lead to epigenomic reprogramming (Cheng *et al*, 2021). It remains unclear what the determinants are that ensure TNF-responsive NFκB signaling results in oscillatory

1 Institute for Quantitative and Computational Biosciences and Department for Microbiology, Immunology and Molecular Genetics, University of California, Los Angeles, CA, USA
2 Department of Medicine, Division of Infectious Diseases, David Geffen School of Medicine and Department for Microbiology, Immunology and Molecular Genetics, University of California, Los Angeles, CA, USA
*Corresponding author. Tel: +1 (310) 7949925; E-mail: ahoffmann@ucla.edu
†These authors contributed equally to this work
‡Present address: Department of Medicine, Brigham and Women's Hospital, Boston, MA, USA
§Present address: Atara Biotherapeutics, Thousand Oaks, CA, USA
¶Present address: DeepKinase Biotechnologies Ltd., Beijing, China

dynamics which distinguish TNF- from PAMP-responsive signaling and minimize alterations to the integrity of the epigenome.

While TNF signaling is typically studied in response to acute exposure or chronically elevated levels (Kalliolias & Ivashkiv, 2016), tonic TNF signaling, that is, the constitutive signaling by TNFR due to baseline secretion of TNF, may also have physiological functions. In the case of type I interferon, tonic signaling promotes antiviral immunity in the lungs (Bradley *et al*, 2019) and contributes to prevention of disease (Gough *et al*, 2012) and maintenance of healthy microbiomes (Marié *et al*, 2021). Both increased and decreased tonic IFN signaling can be harmful (Gough *et al*, 2012). However, less is known about the functional role of tonic TNF signaling, although evidence suggests that TNF is produced spontaneously by a proportion of cells in cell culture, for example, 3% of 3T3 MEFs and 10% of RAW264.7 cells (Pękalski *et al*, 2013). Mutations in the human TNFR extracellular domain result in the auto-inflammatory TNF-receptor-associated periodic syndrome (TRAPS), possibly mediated by aberrant constitutive TNFR signaling and NFκB activation (McDermott *et al*, 1999; Sedger & McDermott, 2014). But whether physiological normal levels of tonic TNF have a functional role remains unexplored.

Here, we investigated the effect of tonic TNF conditioning on the signaling and epigenetic response to acute TNF exposure of macrophages, key immune sentinel cells, responding to pathogens and tissue damage, and coordinating subsequent immune responses (Murray & Wynn, 2011). We found that, in the absence of TNF conditioning, macrophages showed less oscillatory NFκB responses reminiscent of PAMP exposure, which were due to hyper-responsive TNFR signaling functions. The consequence of such subtly exaggerated responses were PAMP-like gene expression responses and epigenomic reprogramming not usually seen in response to acute exposure to the paracrine host cytokine TNF.

Results

Absence of tonic TNF conditioning shifts TNF-induced NFκB responses toward non-oscillatory dynamics

To determine whether naive murine bone-marrow-derived macrophages (BMDMs) grown in sterile conditions may be an adequate model for studying the role of tonic TNF conditioning, we measured the amount of TNF in the cell culture medium conditioned by wild-type (WT) versus $Tnf^{-/-}$ BMDMs. A standard ELISA assay quantified a detectable amount of 6 pg/ml of TNF in WT BMDMs, while $Tnf^{-/-}$ BMDMs did not produce tonic TNF above the blank measurements of the assay (Fig 1A). This represents about 1/30 to 1/10 of the TNF concentration in the medium following 4 or 8 h of stimulation with the TLR2/1-binding pathogen-associated molecular pattern (PAMP) Pam3CSK4 (P3C4) (166 and 78 pg/ml, respectively).

Having established the tonic expression of TNF by BMDMs, we investigated whether baseline NFκB activity was altered by its absence. Using a mouse strain harboring a knockin fluorescently tagged NFκB RelA allele for live-cell fluorescence microscopy to allow visualization of nuclear NFκB localization, indicative of its activity (Adelaja *et al*, 2021), we compared baseline nuclear NFκB fluorescence in unstimulated WT and $Tnf^{-/-}$ cells and found no statistically significant difference (Fig 1B). Electrophoretic mobility shift assays (EMSA) to quantify the presence of DNA-binding NFκB in bulk nuclear lysates also revealed no statistically significant difference between WT and $Tnf^{-/-}$ cells at baseline (Fig 1C).

We next asked whether tonic TNF may have a role in shaping cellular responses to stimulation. Prior studies showed that BMDMs stimulated with extrinsic TNF produce oscillatory dynamics of nuclear NFκB localization (Adelaja *et al*, 2021). Using the same mVenus-RelA mouse strain, we examined NFκB signaling dynamics in response to acute TNF stimulation by live-cell fluorescence microscopy. While NFκB was cytosolic at baseline, upon TNF stimulation, it quickly accumulated in the nucleus in both WT and $Tnf^{-/-}$ cells (Fig 1D). In WT cells, NFκB showed the previously reported heterogeneous oscillatory pattern of activity, translocating out of the nucleus in most cells by 45–60 min, back into the nucleus by 90 min, and out again. In contrast, in $Tnf^{-/-}$ cells, NFκB largely remained inside the nucleus and only showed weak re-localization back into the cytosol in most cells over 150 min (Fig 1D). This lack of oscillations resembled the less oscillatory character of early NFκB activity induced by the PAMP P3C4 (Fig 1D).

Automated image analysis allows for quantification of nuclear NFκB fluorescence in hundreds of single cells per experiment. Heatmap visualization of NFκB signaling in all cells of one experiment and example trajectories confirmed that, while NFκB signaling

Figure 1. Absence of tonic TNF shifts TNF-induced NFκB responses toward non-oscillatory dynamics.

A TNF concentrations in supernatants of WT and $Tnf^{-/-}$ BMDMs unstimulated or stimulated with 10 ng/ml P3C4, quantified by ELISA. (Left) 0, 4, and 8 h time points. (Right) Close-up of 0 h time point. Dashed line indicates mean of blank measurements. Data are represented as mean ± SD of three (4 h, 8 h) or five (0 h) biological replicates using cells from two (4 h, 8 h) or three (0 h) mice. Statistical significance was determined by two-tailed paired-sample *t*-test.

B Nuclear mVenus-RelA fluorescence levels in unstimulated WT and $Tnf^{-/-}$ BMDMs, measured by fluorescence microscopy. Data are represented as mean ± SD of median of all cells in five (WT) or three ($Tnf^{-/-}$) biological replicates. Statistical significance was determined by two-tailed unpaired *t*-test.

C Levels of DNA-binding nuclear NFκB in unstimulated WT and $Tnf^{-/-}$ BMDMs, determined by EMSA. Signal for the NFκB-binding κB-site probe was normalized to NF-Y probe signal. Data are represented as mean ± SD of three biological replicates. Statistical significance was determined by two-tailed paired-sample *t*-test. Measurements for this graph correspond to 0 min time point in Fig EV2C.

D mVenus-RelA localization in WT and $Tnf^{-/-}$ BMDMs stimulated with 10 ng/ml TNF or 10 ng/ml P3C4 over 2.5 h, visualized by fluorescence microscopy. Scale bar represents 50 μm. DIC: differential interference contrast.

E–J Nuclear localization of mVenus-RelA upon stimulation with 10 ng/ml TNF (E–G) or 10 ng/ml P3C4 (H–J), measured over time in WT and $Tnf^{-/-}$ BMDMs by fluorescence microscopy and quantified by automated image analysis. (E, H) Each row of the heatmap represents the NFκB signaling trajectory of one cell. Trajectories are sorted by maximum amplitude. Example trajectories are shown below. Data from a single representative experiment is depicted. (F, I) Indicated dynamic features were calculated from signaling trajectories. Violin plots depict pooled data from 8 (F) or 6 (I) biological replicates (total # of cells: 5,769/5,238 (F), 3,843/3,899 (I)). Marker indicates median of distribution. Statistical significance was determined by Wilcoxon rank-sum test. Number indicates $\log_{10}$(*P*-value). (G, J) Percentage of cells with NFκB trajectories categorized as oscillatory based on a frequency threshold among all responder cells in each experiment. Data are represented as mean ± SD of 8 (G) or 6 (J) biological replicates. Statistical significance was determined by two-tailed paired-sample *t*-test. (F, G) Some replicates for $Tnf^{-/-}$ BMDMs overlap with data in Fig 4G and H.

Source data are available online for this figure.

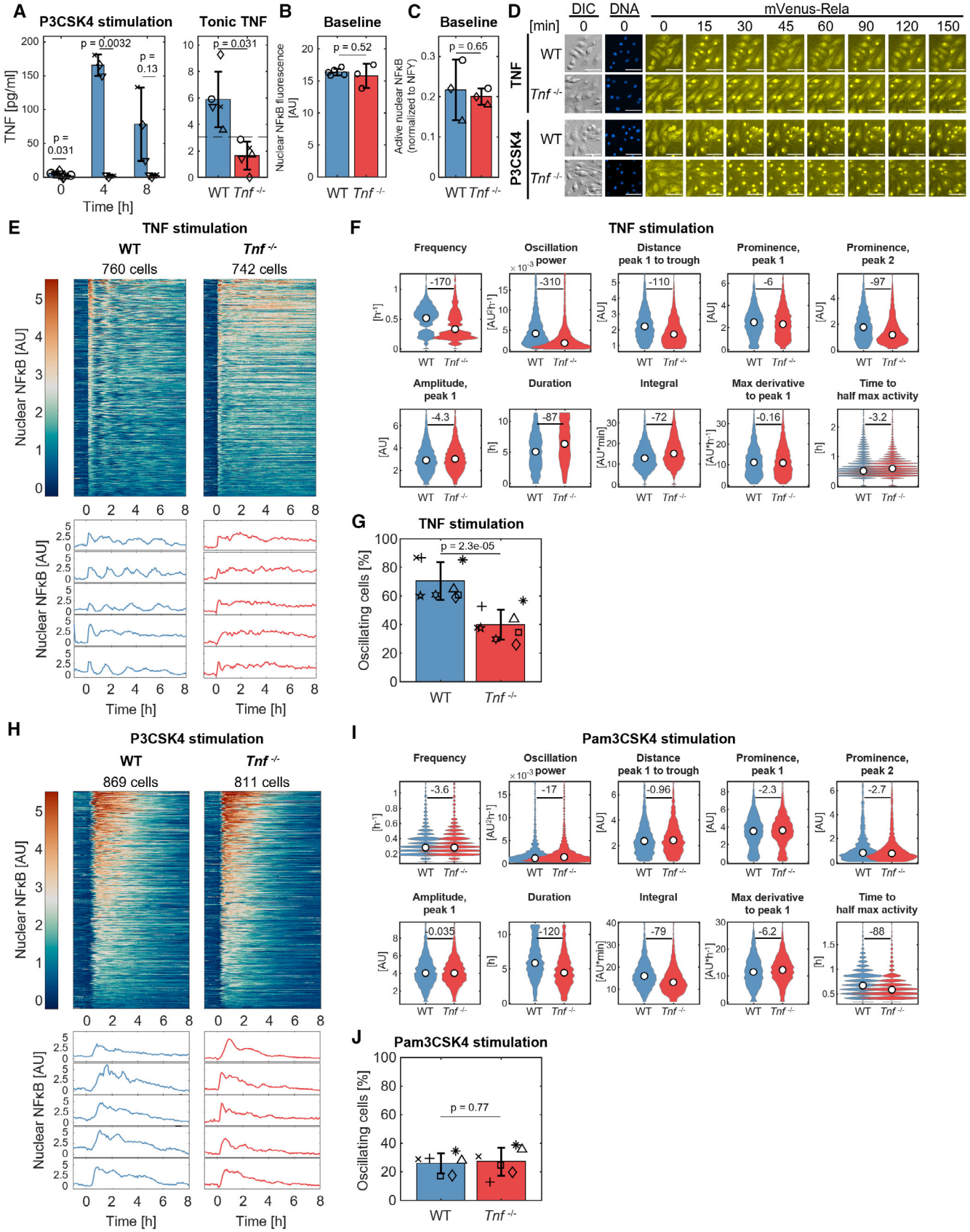

Figure 1.

was oscillatory for up to at least 8 h in many WT cells, it was less oscillatory and more sustained in *Tnf*$^{-/-}$ cells upon TNF stimulation (Fig 1E). In *Tnf*$^{-/-}$ cells, a trough was still seen after the first peak, but it appeared much shallower than in WT cells. Several quantitative metrics of oscillation, such as the frequency and oscillation power of the signal, the amplitude difference between the first peak and the following through, and the prominence of the second peak, were reduced in *Tnf*$^{-/-}$ cells, while other important features that describe NFκB dynamics (Adelaja *et al*, 2021), such as the amplitude of the first peak, the steepness of the first increase, and time required to reach half maximum activity, were less affected. The duration of activity above a certain threshold and the total activity, measured by the integral, were increased in *Tnf*$^{-/-}$ cells, consistent with more sustained NFκB dynamics with shallower troughs between peaks (Fig 1F). Only 40% of *Tnf*$^{-/-}$ cells were categorized as having oscillatory NFκB dynamics, compared to 70% in WT cells, using a Fourier-based analysis (Fig 1G). Thus, in the absence of tonic TNF, NFκB dynamics induced by extrinsic TNF stimulation shift toward non-oscillatory dynamics.

To test whether the NFκB responses to other stimuli are also affected by the loss of endogenous TNF, we analyzed P3C4-induced NFκB dynamics. As expected, most WT cells displayed a sustained, non-oscillatory response, and NFκB dynamics in *Tnf*$^{-/-}$ cells appeared very similar but had shorter duration (Fig 1D and H). Indeed, quantitative analysis of the trajectories confirmed that metrics of oscillations, such as frequency, oscillation power, and peak prominence, were not reduced in *Tnf*$^{-/-}$cells (Fig 1I, top row). In accordance with the literature (Caldwell *et al*, 2014), the duration of signaling induced solely by the MyD88 adaptor was shorter in *Tnf*$^{-/-}$ cells (presumably due to the lack of autocrine signaling by newly synthesized TNF), while the amplitude was not altered, resulting in lower total activity (integral), and a shorter time to half maximum activity (Fig 1I, bottom row). The proportion of cells with oscillatory NFκB dynamics was not significantly altered in *Tnf*$^{-/-}$ compared to WT cells (27% versus 26%; Fig 1J). Overall, the absence of tonic TNF affects the oscillatory characteristics of TNF-induced NFκB responses more than those of P3C4-induced responses.

Supplementing the *Tnf*$^{-/-}$ BMDMs culture with a low concentration of exogenous TNF might mimic the effects of tonic endogenous TNF signaling and restore oscillatory NFκB dynamics. While 6 pg/ml tonic TNF was measured by ELISA, the local concentration at the cellular membrane is likely higher. Even culturing *Tnf*$^{-/-}$ cells with 250 pg/ml TNF for 96 h before stimulation with 10 ng/ml TNF showed only a partial restoration of wild-type dynamics: the NFκB response to TNF decreased in amplitude of first peak, duration of response, total activity (integral), and steepness of the first increase (Fig EV1A and B). Peak prominence and amplitude difference between the first peak and the following trough were decreased, presumably due to the difference in amplitude of the signal. We also found a small increase in the median frequency (Fig EV1B) and oscillatory proportion (30% without TNF pre-treatment versus 39% with TNF pre-treatment; $P = 0.062$; Fig EV1C) in the NFκB trajectories in *Tnf*$^{-/-}$ cells pre-treated with a low dose of TNF. These results indicate that providing exogenous TNF does not fully mimic the physiological effect of tonic TNF signaling. In a co-culture of *Tnf*$^{-/-}$ cells with 85% non-fluorescent WT cells, which might provide exposure to both soluble TNF (sTNF) and transmembrane TNF (tmTNF) via intercellular contact, oscillation power and prominence of the first peak increased slightly (Fig EV1D and E), but the percentage of cells with oscillatory trajectories was not detectably altered (23% in absence of WT cells versus 23% in co-culture with WT cells; $P = 0.43$; Fig EV1F). This suggests that paracrine supply of tonic TNF (sTNF or tmTNF) does not recapitulate the WT phenotype.

Considering mechanisms controlling the oscillatory content in TNF-induced NFκB dynamics

Upon signaling from the upstream TNF receptor, IKK is activated and targets IκBα, which binds to NFκB and prevents it from entering the nucleus, for degradation, allowing free NFκB to enter the nucleus. There, NFκB induces gene expression, including expression of IκBα. Once produced, IκBα protein can bind to nuclear (and cytosolic) NFκB, bringing it from the nucleus into the cytoplasm and sequestering it there (Fig 2A; Mitchell *et al*, 2016). Thus, IκBα induction may mediate post-induction repression of NFκB activity. Sustained low or intermediate IKK activity then allows for another round of IκBα degradation and nuclear NFκB activity, resulting in oscillatory dynamics. However, sustained high IKK activity neutralizes the feedback loop by quickly degrading newly synthesized IκBα before it can effectively inhibit NFκB activity, resulting in non-oscillatory dynamics (Adelaja *et al*, 2021). Thus, the oscillatory content of NFκB dynamics is determined by both the NFκB-responsive IκBα-negative feedback loop and the level of IKK activity.

To elucidate the molecular mechanism(s) responsible for the diminished oscillatory content in the absence of tonic TNF conditioning, we first investigated the strength of feedback control through NFκB-responsive IκBα expression, which is essential for oscillatory NFκB responses. Decreased IκBα feedback, especially in the first hour after stimulation, would result in reduced post-induction inhibition of NFκB and, hence, a more sustained NFκB response with decreased prominence of the activity trough at 45–60 min. Early induction of IκBα mRNA upon TNF stimulation was very similar in WT and *Tnf* $^{-/-}$ cells with peak expression at 60 or 70 min in WT and *Tnf*$^{-/-}$ cells, respectively (Fig 2B). IκBα mRNA levels decreased both in WT and *Tnf* $^{-/-}$ cells from 70 to 100 min of TNF stimulation and increased slightly from 100 to 120 min, corresponding to the preceding changes in nuclear levels of NFκB (Fig 1E). The post-peak decrease was smaller in *Tnf* $^{-/-}$ cells, resulting in IκBα mRNA levels in *Tnf* $^{-/-}$ cells that were 1.4× – 1.6× of WT levels after 1 h of stimulation (Fig 2B). Presumably, this was due to the more sustained presence of NFκB in the nucleus, that is, decreased prominence of the first oscillatory trough, in *Tnf* $^{-/-}$ cells (Fig 1E). Thus, there is no impairment of the IκBα feedback loop in the absence of tonic TNF conditioning.

Upstream of the IκBα-NFκB feedback circuit, the magnitude of IKK activity is a key determinant of the oscillatory character of NFκB activity (Fig 2A; Adelaja *et al*, 2021). If IKK activity is high, newly produced IκBα is quickly targeted for degradation before it can translocate to the nucleus to strip NFκB off the DNA. Thus, diminished oscillatory content in NFκB dynamics in the absence of tonic TNF might be mediated by increased IKK activity. We determined levels of phosphorylated IKK by western blotting as an indicator of its activity (Fig 2C and D). In WT cells, IKK phosphorylation peaked at 5 min post-TNF stimulation and decreased to low, near-baseline levels by 30 min. Rapid cyclic

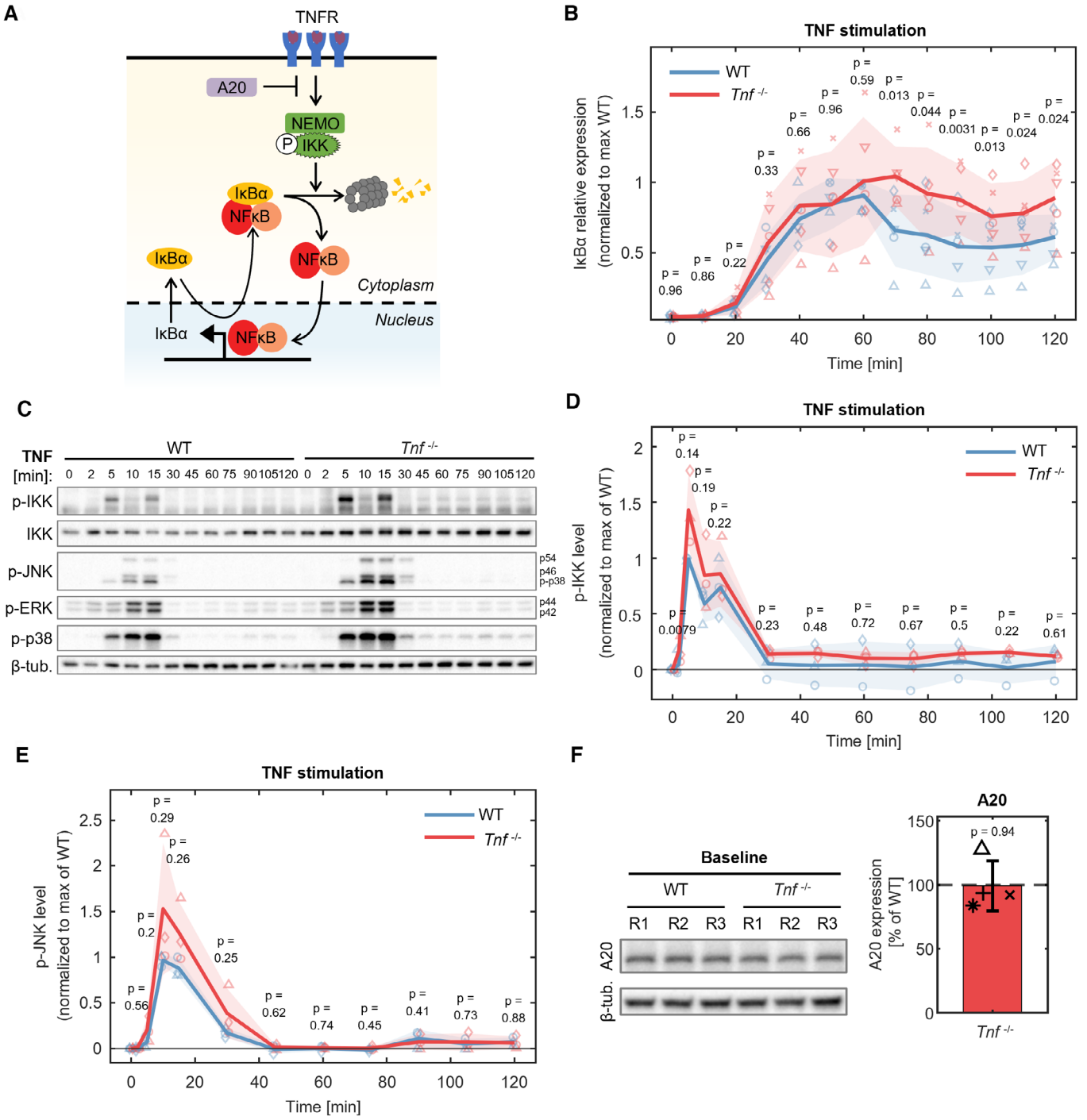

Figure 2.

regulation of this kinase through phosphorylation, dephosphorylation, and re-phosphorylation between 5 and 15 min could be observed (Behar & Hoffmann, 2013; Fig 2C). In *Tnf*$^{-/-}$ cells, IKK phosphorylation followed a similar temporal pattern but was slightly increased compared to WT across all time points, to 3.6×, 1.4×, 1.4×, and 1.2× of WT levels at 2, 5, 10, and 15 min, and to 1.7–8.9× of WT levels from 30 to 120 min, although many of these differences were not statistically significant (Fig 2D). An increase in IKK activity in *Tnf*$^{-/-}$ cells at the later phase is especially relevant, as these time points have the potential to influence the oscillatory character of the NFκB responses. Between 30 and 120 min, IKK activity in *Tnf*$^{-/-}$ cells ranged from 10 to 15% of peak WT IKK activity, while in WT cells, it ranged from 2 to 7%. Total IKK levels were not increased in *Tnf*$^{-/-}$ cells compared to WT (Fig EV2A). The possible increase in IKK activity corresponds to a similar, statistically not significant increase in nuclear NFκB DNA-binding activity to 1.1–1.2× at 30, 60, 90, and 120 min, measured by electrophoretic mobility shift assay (EMSA; Fig EV2B and C).

Figure 2. Potential mechanisms controlling the oscillatory content in TNF-induced NFκB dynamics.

A Schematic of the signaling network mediating TNF-induced NFκB oscillations. Signaling by TNF receptors activates IKK, which targets IκBα for degradation by the proteasome. IκBα degradation releases NFκB, which will accumulate in the nucleus and bind DNA. NFκB-responsive *Nfkbia* gene expression leads to increased IκBα levels, which travels to the nucleus to bind NFκB and shuttle it out of the nucleus. If IKK activity persists, multiple rounds of NFκB nuclear translocation and activity are possible. The ubiquitin-chain-regulating protein A20 inhibits TNF-induced signaling at multiple steps.

B IκBα mRNA expression in WT and $Tnf^{-/-}$ BMDMs stimulated with 10 ng/ml TNF over 2 h, determined by RT–qPCR. IκBα expression was normalized to GAPDH expression and then to maximum WT value in each time-course replicate. Data are represented as mean ± SD of five biological replicates. Statistical significance was determined by two-tailed paired-sample *t*-test for each time point. Some replicates for $Tnf^{-/-}$ BMDMs overlap with data in Fig 4D.

C–E Phosphorylation of IKK, JNK, ERK, and p38 and total IKK levels in WT and $Tnf^{-/-}$ BMDMs stimulated with 10 ng/ml TNF over 2 h, determined by SDS–PAGE followed by western blotting. (C) One of three representative experiments is shown. (D, E) For quantification of p-IKK (D) and p-JNK p54 (E) levels, basal levels (0 min) were deducted per genotype before normalizing to maximum WT value in each experiment. Data are represented as mean ± SD of three biological replicates. Statistical significance was determined by two-tailed paired-sample *t*-test for each time point.

F A20 protein levels in unstimulated WT and $Tnf^{-/-}$ BMDMs, determined by SDS–PAGE followed by western blotting. (Left) Western blot of A20 and β-tubulin (β-tub.) from one representative experiment with three culture replicates (R1-R3). (Right) For quantification, in each experiment, A20 levels from three culture replicates were averaged, and A20 levels in $Tnf^{-/-}$ cells were expressed as percentage of A20 levels in WT cells. Data are represented as mean ± SD of four biological replicates. Statistical significance was determined by two-tailed one-sample *t*-test using a hypothesis mean of 100.

Source data are available online for this figure.

In addition to IKK-NFκB activation, MAPK cascades are activated downstream of TNFR and TLR signaling. To determine whether these other pathways were also affected by the absence of tonic TNF, we determined levels of phosphorylated JNK, ERK, and p38, indicative of their activation, by western blotting (Fig 2C). Levels of JNK phosphorylation peaked at 10 min after TNF stimulation and declined to baseline levels by 45 min in both WT and $Tnf^{-/-}$ cells. They appeared slightly increased in $Tnf^{-/-}$ cells compared to WT at 5, 10, 15, and 30 min to 2.8×, 1.6×, 1.4×, and 2.3× of WT levels, although the differences were not statistically significant (Fig 2E). ERK and p38 MAPK activation by TNF did not appear affected by the absence of tonic TNF: phosphorylation of the kinases was similar in WT and $Tnf^{-/-}$ cells. In both genotypes, both kinases showed a sharp increase in phosphorylation upon cell stimulation, peaking at 10 min and decreasing to below baseline (p-ERK) and almost to baseline (p-p38) by 30–45 min (Fig EV2D and E). In sum, our data are consistent with elevated TNF-responsive IKK and JNK MAPK activation when tonic TNF signaling is absent, while ERK and p38 MAPK activation are not affected.

We next aimed to determine the cause of hyper-responsiveness in the absence of tonic TNF conditioning. A20 is a TNF-inducible protein that inhibits signaling at multiple steps downstream of the TNF receptor and may fine-tune NFκB responses when expressed (Fig 2A; Wertz *et al*, 2004; Werner *et al*, 2008; Catrysse *et al*, 2014). If A20 expression was decreased at baseline in the absence of tonic TNF, this could increase pathway activity, resulting in increased IKK activity and less oscillatory NFκB responses. However, comparing baseline A20 protein levels in WT and $Tnf^{-/-}$ cells by western blotting, we found no difference (Fig 2F). Thus, A20 does not appear to be involved in the altered NFκB dynamics in $Tnf^{-/-}$ cells.

TNF receptor turnover and signaling mechanisms control the oscillatory content in NFκB dynamics

We next investigated whether TNF receptor turnover and signaling functions, which may be affected by tonic TNF, could be determinants of the oscillatory content of TNF-induced NFκB dynamics. We leveraged a mathematical model of TNF-induced NFκB activation, which delineates 13 biochemical reactions that describe the interactions of the TNFR with the ligand TNF and the downstream signaling complex C1 (following recruitment of TRAF2, TRADD, and RIP1K; Fig 3A; Adelaja *et al*, 2021). A parameter scan (using multiplier steps of $10^{0.1}$ or $10^{-0.1}$) determined that 5 of the 13 biochemical reactions sensitively affected the oscillatory content of TNF-induced NFκB dynamics: the TNFR expression rate (k54), the internalization/decay rate of receptors bound to ligand and signaling complex (k61), the activation/inactivation (k62, k63) of the signaling complex, and its ability to activate TAK1 and IKK (k65; Fig 3A).

To simulate heterogenous single-cell NFκB responses, the five sensitive parameters were sampled individually or in pairwise combinations from a log-normal distribution of parameter values with $\sigma = \ln(2)/3$ (Cheng *et al*, 2015). For "WT" cells, the means of the distributions were placed at the original parameter values. For "$Tnf^{-/-}$" cells, the means of the five sensitive parameters were shifted by a factor of $10^{0.1}$ or $10^{-0.1}$ (Fig EV3A and B). When sampling any of the five parameters individually, both simulated "WT" and "$Tnf^{-/-}$" cells showed predominantly oscillatory responses, with moderate heterogeneity in amplitude and period of the oscillation (Figs 3B and EV3C, row 1, 2). While 100% of simulated "WT" cells were categorized as oscillatory for all five individual parameter samplings, "$Tnf^{-/-}$" cells were oscillatory at a slightly lower percentage (96–97%; Figs 3B and EV3C, row 3), with higher trough amplitudes (Figs 3B and EV3C, row 1,2). The trajectories in "$Tnf^{-/-}$" cells had shifted oscillation power distributions with lower medians (Figs 3B and EV3C, row 4). When sampling pairwise combinations of the five sensitive parameters, the heterogeneity of the simulated NFκB responses increased (Figs 3B and EV3C, row 1,2). All parameter combinations showed a lower percentage of cells with oscillatory NFκB responses in "$Tnf^{-/-}$" cells (52–55%) than in "WT" cells (60–66%; Figs 3B and EV3C, row 3) and higher trough amplitudes (Figs 3B and EV3C, row 1,2). The oscillation power distributions showed more heterogeneity than in the single parameter sampling with a decrease in oscillation power in "$Tnf^{-/-}$" cells compared to "WT" cells (Figs 3B and EV3C, row 4).

Examining the average IKK activity in these simulations revealed a sharp peak at 6–7 min after stimulation with a fast decrease to lower, but above baseline levels by 45–50 min, followed by a slow decline toward baseline levels over 7 h (Figs 3C and EV3D). IKK activity was increased in simulated "$Tnf^{-/-}$" cells compared to "WT" cells in all individual and pairwise parameter samplings by 1.2–1.6×, in agreement with experimental results. These results suggest that the subtle, statistically not significant increases in IKK

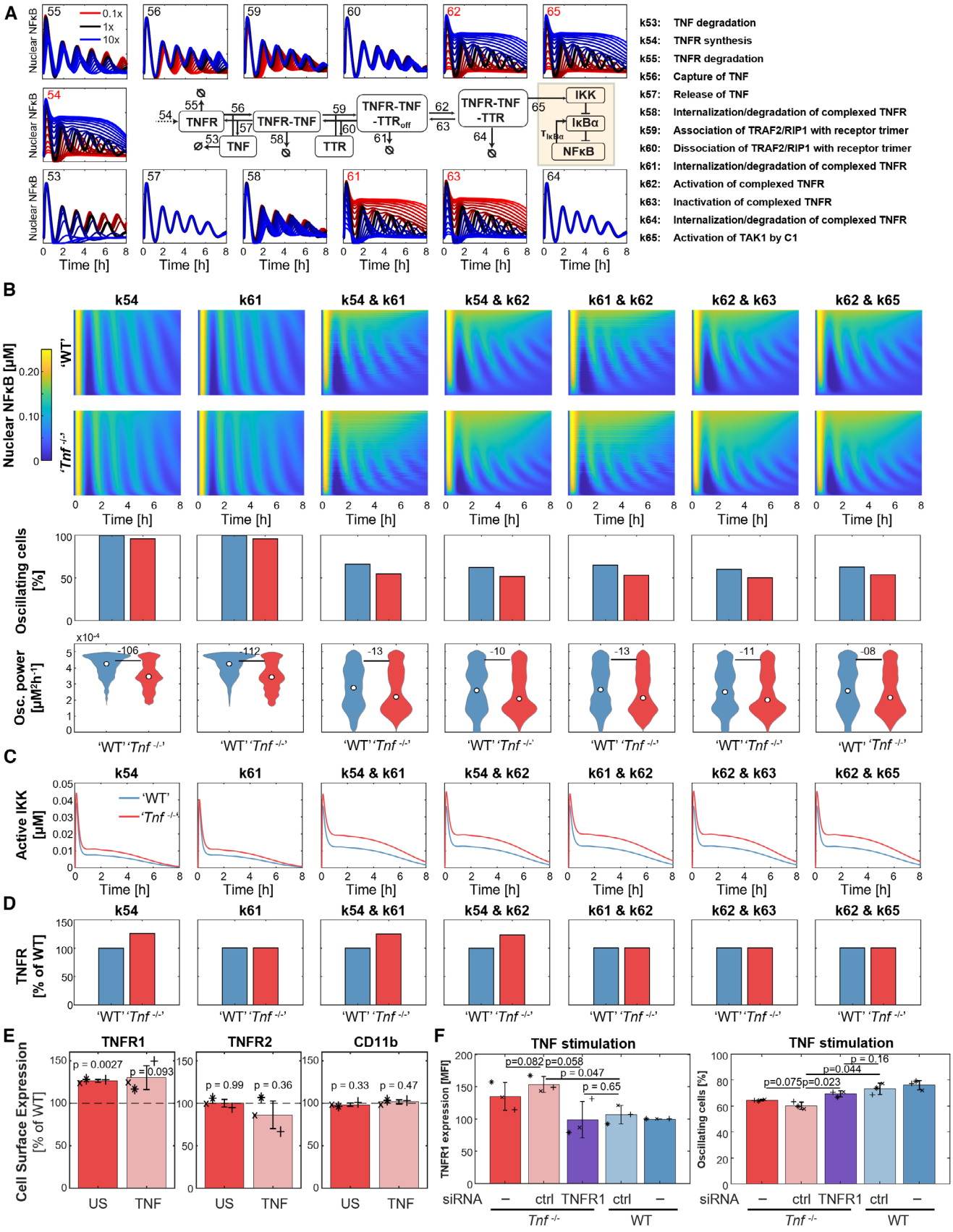

Figure 3.

Figure 3. Mechanisms regulating TNF receptor turnover and signaling control the oscillatory content in TNF-induced NFκB dynamics.

A Parameter scan (left) of listed reaction parameters (right) in the TNF receptor module (white background) of the NFκB signaling network model and simplified depiction of the NFκB core module (yellow background). Graphs depict nuclear NFκB dynamics over 8 h with increased (blue, $10^{0.1}\times$ to $10^{1}\times$) and decreased (red, $10^{-0.1}\times$ to $10^{-1}\times$) parameter values in 10 steps each (linear on log scale) from the original model parameters (1×). Parameter indices that allow a shift of simulated TNF-induced NFκB oscillations to less oscillatory dynamics are labeled in red.

B Simulated single-cell nuclear NFκB dynamics upon TNF stimulation over 8 h (heatmaps) sorted by maximum amplitude in "WT" and "*Tnf*$^{-/-}$" cells (row 1, row 2). Parameters determined in (A) to allow decrease in oscillatory character of NFκB dynamics were distributed for sampling (sampled parameter indicated in heatmap heading). NFκB dynamics in simulated *Tnf*$^{-/-}$ cells were modeled by shifting the mean of the parameter distributions by $10^{0.1}$ or $10^{-0.1}$ (see Fig EV3A). Indicated pairs of parameters were also sampled. Percentage of cells with oscillatory NFκB trajectories among all simulated responder cells (row 3) and oscillation power of simulated NFκB trajectories (row 4) are shown below. A total of 2,000 cells were simulated. Marker indicates median of distribution. Statistical significance was evaluated by Kolmogorov–Smirnov test. Number indicates $\log_{10}$(*P*-value). Results for other parameters and parameter combinations that can mediate less oscillatory responses are shown in Fig EV3C.

C Simulated average IKK activity over 8 h in mathematical models of TNF-induced NFκB dynamics in "WT" and "*Tnf*$^{-/-}$" cells, as in (B).

D Simulated mean TNF receptor levels at steady state in mathematical models of TNF-induced NFκB dynamics in "WT" and "*Tnf*$^{-/-}$" cells, as in (B).

E TNF receptor 1 (TNFR1, left), TNF receptor 2 (TNFR2, center), and CD11b (right) cell surface expression in *Tnf*$^{-/-}$ compared to WT BMDMs unstimulated or stimulated for 30 min with 10 ng/ml TNF, measured by flow cytometry. Per experiment, median fluorescence intensity average of three culture replicates in *Tnf*$^{-/-}$ cells is expressed as percent of expression in WT cells. Data are represented as mean ± SD of three biological replicates. Statistical significance was determined by two-tailed one-sample *t*-test using a hypothesis mean of 100.

F (Left) TNF receptor 1 (TNFR1) cell surface expression at baseline in BMDMs pre-treated with TNFR1 siRNA, control (ctrl) siRNA, or untreated (–). Median fluorescence intensity is expressed as percent of expression in untreated WT cells. (Right) Percentage of cells with oscillatory NFκB activity (measured by fluorescence microscopy) among all responder cells upon indicated siRNA pre-treatment and stimulation with 10 ng/ml TNF. Per condition, 1,032–1,484 responding cells were analyzed. (Left, right) Data are represented as mean ± SD of three biological replicates. Statistical significance was determined by one-tailed paired-sample *t*-test. Heatmaps of NFκB trajectories from one biological replicate are show in Fig EV3G.

Source data are available online for this figure.

activity experimentally observed in *Tnf*$^{-/-}$ cells (1.4× of WT at peak activity and 1.7× at 2 h; Fig 2D) may contribute to the reduction in oscillatory content in NFκB dynamics when tonic TNF conditioning is absent.

Next, we examined the role of TNF receptor cell surface expression levels. In any simulations where k54 was increased, either individually or in combination with one of the other parameters, mean TNFR surface levels were elevated by 123–127% of "WT" levels (Figs 3D and EV3E). Thus, experimentally, we determined cell surface levels of TNFR1 and TNFR2 at baseline and after 30 min of TNF stimulation by flow cytometry. *Tnf*$^{-/-}$ cells had higher baseline TNFR1 levels than WT cells (126% of WT cells, *P*-value of 0.0027; Fig 3E, left). Even after much of the receptor was internalized upon TNF stimulation (Fig EV3F, left), the cell surface level appeared to be higher in *Tnf*$^{-/-}$ than in WT cells (130% of WT, *P*-value of 0.093; Fig 3E, left). Baseline TNFR2 surface level was not altered in *Tnf*$^{-/-}$ cells (100% of WT; Figs 3E and EV3F, center). As a control, CD11b cell surface levels were unaltered by TNF deficiency or by TNF stimulation (Figa 3E and EV3F, right). To provide further evidence for a causal relationship between increased TNFR1 surface expression and reduced percentage of oscillatory NFκB trajectories in the absence of tonic TNF, we reduced baseline TNFR1 surface expression in *Tnf* $^{-/-}$ BMDMs to levels similar to WT using TNFR1 siRNA-mediated gene silencing (Fig 3F, left). Compared to control siRNA-transfected *Tnf* $^{-/-}$ cells (60% oscillatory NFκB trajectories), *Tnf* $^{-/-}$ cells with reduced TNFR1 levels had a higher percentage of oscillatory NFκB trajectories (69%, $P = 0.023$), with control siRNA-transfected WT cells having 73% oscillatory NFκB trajectories (Fig 3F, right). Thus, reducing TNFR1 expression to WT levels in *Tnf* $^{-/-}$ cells partially rescues the oscillatory NFκB dynamics.

In sum, the combination of mathematical modeling and experimental studies suggests that tonic TNF conditioning may promote oscillatory NFκB dynamics in response to TNF by affecting a number of biochemical reactions that control the turnover, recycling, and signaling functions of the TNF receptor. Several subtle changes, often near the limit of experimental detection, may combine to have a surprisingly pronounced effect on NFκB oscillations. This illustrates in turn that live cell imaging of NFκB signaling is an exquisitely sensitive assay to probe the cellular state.

Strengthening the IκBα-negative feedback on NFκB partially restores TNF-induced NFκB oscillations

As the computational modeling analysis suggested that the reduced oscillatory content of NFκB responses in the absence of tonic TNF conditioning may be mediated by increased IKK activity, we aimed to provide further experimental evidence to support this conclusion. If the excess IKK activity observed in the absence of tonic TNF neutralizes the IκBα-negative feedback loop and thus diminishes post-activation repression of NFκB and NFκB oscillations, we reasoned that strengthening IκBα feedback control may compensate and restore NFκB oscillations. This may be illustrated by model simulations in which IKK-responsive NFκB is elevated to increase expression of and negative feedback by IκBα. Applying a 1.25× increase in NFκB to a "*Tnf* $^{-/-}$" model (sampling k54 and k61 distributions as in Figs 3B and EV3C, column 3), we found that average NFκB-responsive IκBα mRNA expression was increased to levels higher than in the *Tnf* $^{-/-}$ model already at early time points as expected (Fig 4A). As a result, NFκB oscillations were indeed restored (Fig 4B). Analysis of these simulations revealed elevated oscillatory content in the 1.25× NFκB condition with an increase in oscillation power and the percentage of cells with oscillatory NFκB trajectories (85% versus 57% in controls; Fig 4C).

To experimentally test the model predictions, we utilized a genetic perturbation that renders more cellular NFκB responsive to TNF. The IκBsome is a protein complex consisting of p105 and p100 subunits, which traps NFκB. It is not responsive to the canonical IKK pathway (Basak *et al*, 2007; Savinova *et al*, 2009; Shih *et al*, 2009). By genetic removal of the nfkb2/p100 subunit, the

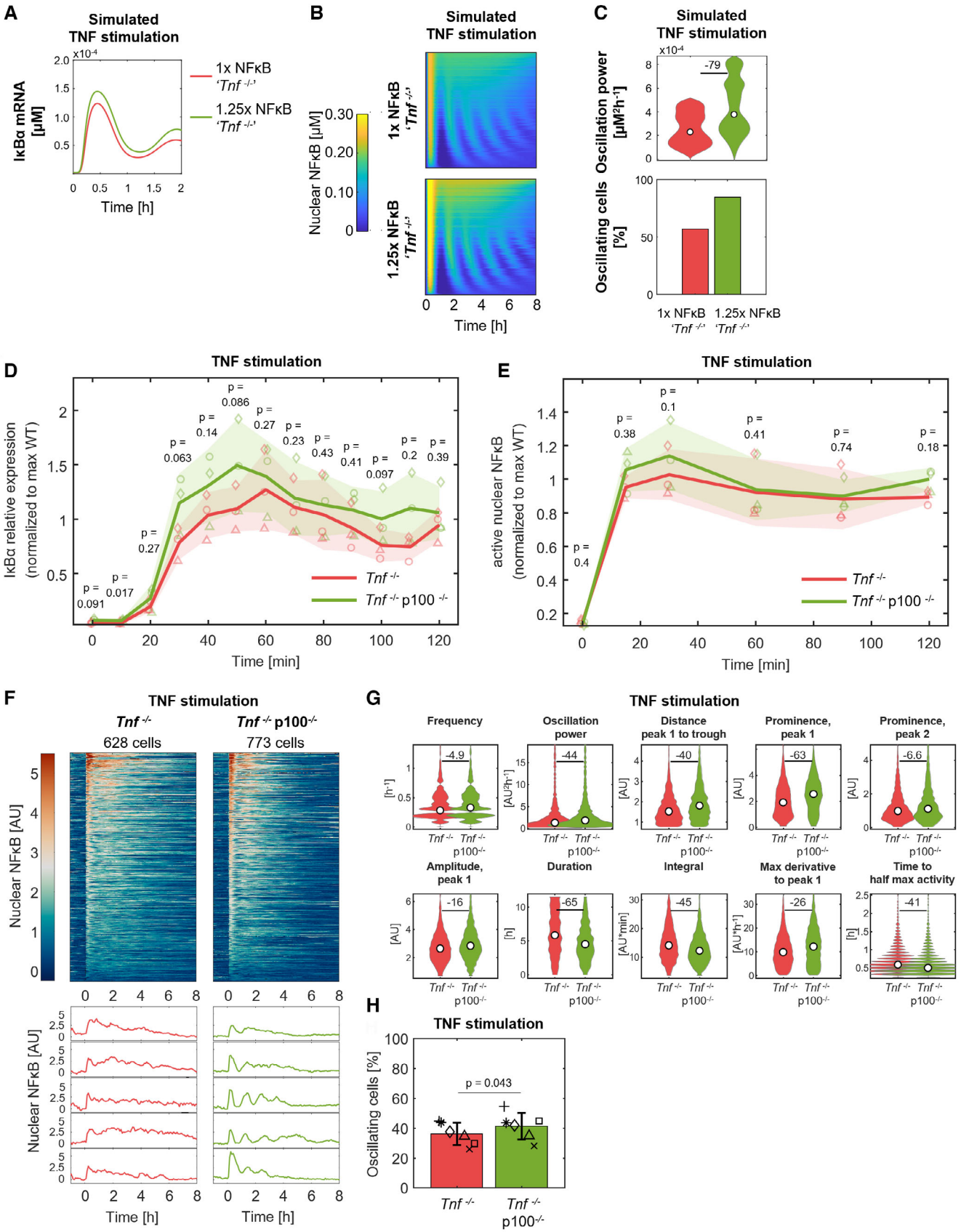

Figure 4.

Figure 4. Strengthening the IκBα-negative feedback on NFκB partially restores TNF-induced NFκB oscillations.

A Simulated average Iκbα mRNA expression level over 2 h in mathematical models of TNF-induced NFκB pathway signaling in "$Tnf^{-/-}$" model and "$Tnf^{-/-}$" model with 1.25× total NFκB levels. Parameters k54 and k61 are sampled.

B Simulated single-cell NFκB dynamics upon TNF stimulation over 8 h in "1× NFκB, $Tnf^{-/-}$" and "1.25× NFκB, $Tnf^{-/-}$" models, as in (A).

C Oscillation power of simulated trajectories and percentage of cells with oscillatory NFκB trajectories among all simulated responder cells in "1× NFκB, $Tnf^{-/-}$" and "1.25× NFκB, $Tnf^{-/-}$" models, as in (A). A total of 1,000 cells were simulated. Marker indicates median of distribution. Statistical significance was evaluated by Kolmogorov–Smirnov test. Number indicates $\log_{10}$(*P*-value).

D IκBα mRNA expression in $Tnf^{-/-}$ and $Tnf^{-/-}$p100$^{-/-}$ BMDMs stimulated with 10 ng/ml TNF over 2 h, determined by RT–qPCR. IκBα expression was normalized to GAPDH expression and then to maximum WT value also obtained with each replicate. Data are represented as mean ± SD of three biological replicates. Statistical significance was determined by two-tailed paired-sample *t*-test for each time point. Data for $Tnf^{-/-}$ BMDMs are also included in Fig 2B.

E Levels of nuclear NFκB DNA-binding activity in $Tnf^{-/-}$ and $Tnf^{-/-}$p100$^{-/-}$ BMDMs stimulated with 10 ng/ml TNF over 2 h, determined by EMSA. Quantification of the NFκB-DNA complex was normalized to the quantified NFY-DNA complex, and then to maximum WT value also obtained with each replicate. Data are represented as mean ± SD of three biological replicates. Statistical significance was determined by two-tailed paired-sample *t*-test for each time point. Data for $Tnf^{-/-}$ BMDMs are also shown in Fig EV2C.

F–H Nuclear localization of mVenus-RelA upon stimulation with 10 ng/ml TNF was measured over time by fluorescence microscopy in $Tnf^{-/-}$ and $Tnf^{-/-}$p100$^{-/-}$ BMDMs and quantified by automated image analysis. (F) Each row of the heatmap represents the NFκB signaling trajectory of one cell. Trajectories are sorted by maximum amplitude. Example trajectories are shown below. Data from a single representative experiment are depicted. (G) Indicated dynamic features were calculated from signaling trajectories. Violin plots depict pooled data from six biological replicates (total # of cells: 4,030/4,133). Marker indicates median of distribution. Statistical significance was determined by Wilcoxon rank-sum test. Number indicates $\log_{10}$(*P*-value). (H) Percentage of cells with NFκB trajectories was categorized as oscillatory based on a frequency threshold among all responder cells in each experiment. Data are represented as mean ± SD of six biological replicates. Statistical significance was determined by one-tailed paired-sample *t*-test. (G, H) Data for $Tnf^{-/-}$ BMDMs is also included in Fig 1F and G.

Source data are available online for this figure.

IκBsome complex collapses (Yılmaz *et al*, 2014), freeing more NFκB to associate with canonical IκB proteins. Upon stimulus-induced degradation of canonical IκB proteins, the additional NFκB can translocate to the nucleus to drive a stronger IκBα-negative feedback loop. Therefore, to mimic the "*Tnf* $^{-/-}$ with 1.25× NFκB" model conditions, we bred *Tnf* $^{-/-}$ p100$^{-/-}$ mice to increase the amount of stimulus-responsive NFκB and the strength of the IκBα-negative feedback in *Tnf* $^{-/-}$ background. Indeed, we found that while *Tnf* $^{-/-}$ BMDMs showed good NFκB-responsive IκBα induction, *Tnf* $^{-/-}$p100$^{-/-}$ BMDMs showed a further, small, statistically non-significant increase in TNF-induced IκBα mRNA expression, especially at 20–50 min (starting before the induction peak is reached at 50 or 60 min) and 100–110 min (at a trough in the induction dynamic) after stimulation (1.3–1.5× of mRNA levels in $Tnf^{-/-}$ cells; Fig 4D). In addition, levels of nuclear NFκB DNA-binding activity, determined by EMSA, appeared slightly increased in *Tnf* $^{-/-}$p100$^{-/-}$ BMDMs to 1.1× at 15, 30, and 120 min after TNF stimulation (Figs 4E and EV4). In *Tnf* $^{-/-}$p100$^{-/-}$ BMDMs, nuclear NFκB decreased more distinctly from its peak levels at 30 min to 60 and 90 min (where levels were comparable to $Tnf^{-/-}$ cells) and increased more distinctly to 120 min.

Next, we analyzed single-cell mVenus-RelA NFκB signaling upon TNF stimulation in *Tnf* $^{-/-}$p100$^{-/-}$ cells by live-cell microcopy. Heatmap visualization of NFκB signaling in all cells of one experiment and example trajectories showed that, compared to $Tnf^{-/-}$ cells, *Tnf* $^{-/-}$p100$^{-/-}$ cells had more oscillatory trajectories, with more prominent troughs after the first peak (Fig 4F). Quantitative metrics of oscillations, especially oscillation power, the amplitude difference between the first peak and the following trough, and the prominence of the first peak were increased *Tnf* $^{-/-}$p100$^{-/-}$ cells, while duration above a certain threshold and total activity were reduced (Fig 4G). The percentage of cells categorized as having oscillatory NFκB trajectories increased to 41% in *Tnf* $^{-/-}$p100$^{-/-}$ cells from 36% in $Tnf^{-/-}$ cells ($P = 0.04$; Fig 4H). Thus, modeling and experimental data suggest that the reduction in oscillations in *Tnf* $^{-/-}$ cells results from increased IKK activity and may be rescued by increasing IκBα feedback. In sum, these results provide functional evidence that tonic TNF-conditioning reduces stimulus-responsive IKK activity in response to TNF stimulation, thereby ensuring that TNF-induced NFκB dynamics are largely oscillatory.

Tonic TNF conditioning controls TNF-induced gene expression and *de novo* enhancer formation

The duration and oscillatory content of nuclear NFκB activity control inflammatory gene expression and *de novo* enhancer formation (Sen *et al*, 2020; Cheng *et al*, 2021). Therefore, we investigated whether tonic TNF conditioning, which safeguards the TNF-specific characteristics of NFκB dynamics, affects gene expression responses and *de novo* enhancer formation.

First, we measured single-cell gene expression using the Fluidigm system in WT and $Tnf^{-/-}$ BMDMs stimulated with TNF or P3C4 for 4 h. In WT cells, these stimuli resulted in transcriptomes that were substantially separated on UMAP dimensionality reduction plots and a PCA plot of the first two components (Fig 5A and B). In contrast, the transcriptomes of TNF- and P3C4-stimulated $Tnf^{-/-}$ cells were less distinguishable: On the UMAP plot, the two $Tnf^{-/-}$ populations overlapped more than the WT populations (Fig 5A); and on the PCA plot, the population of TNF-stimulated $Tnf^{-/-}$ cells appeared shifted compared to WT to overlap with P3C4-stimulated *Tnf* $^{-/-}$ cells (Fig 5B). This suggests that the lack of tonic TNF conditioning changes gene expression induced by the host cytokine TNF to be more similar to gene expression responses to the PAMP P3C4. Indeed, the average pairwise transcriptome distances (calculated using the first 20 PCA components) between TNF- and P3C4-stimulated cells were smaller in $Tnf^{-/-}$ than in WT cells (Fig 5C). Moreover, in $Tnf^{-/-}$ cells, the fold changes between P3C4- and TNF-induced expression of the majority of the top 50 genes differentially expressed in P3C4 vs. TNF stimulated WT cells were reduced (Fig 5D).

Among 216 genes significantly induced over mock by either P3C4 or TNF stimulation in WT cells, 10 showed significantly higher expression in $Tnf^{-/-}$ cells versus WT cells upon TNF stimulation, all of which have been reported as NFκB-dependent genes (Rouillard *et al*, 2016; Cheng *et al*, 2017; Wu *et al*, 2022), while the

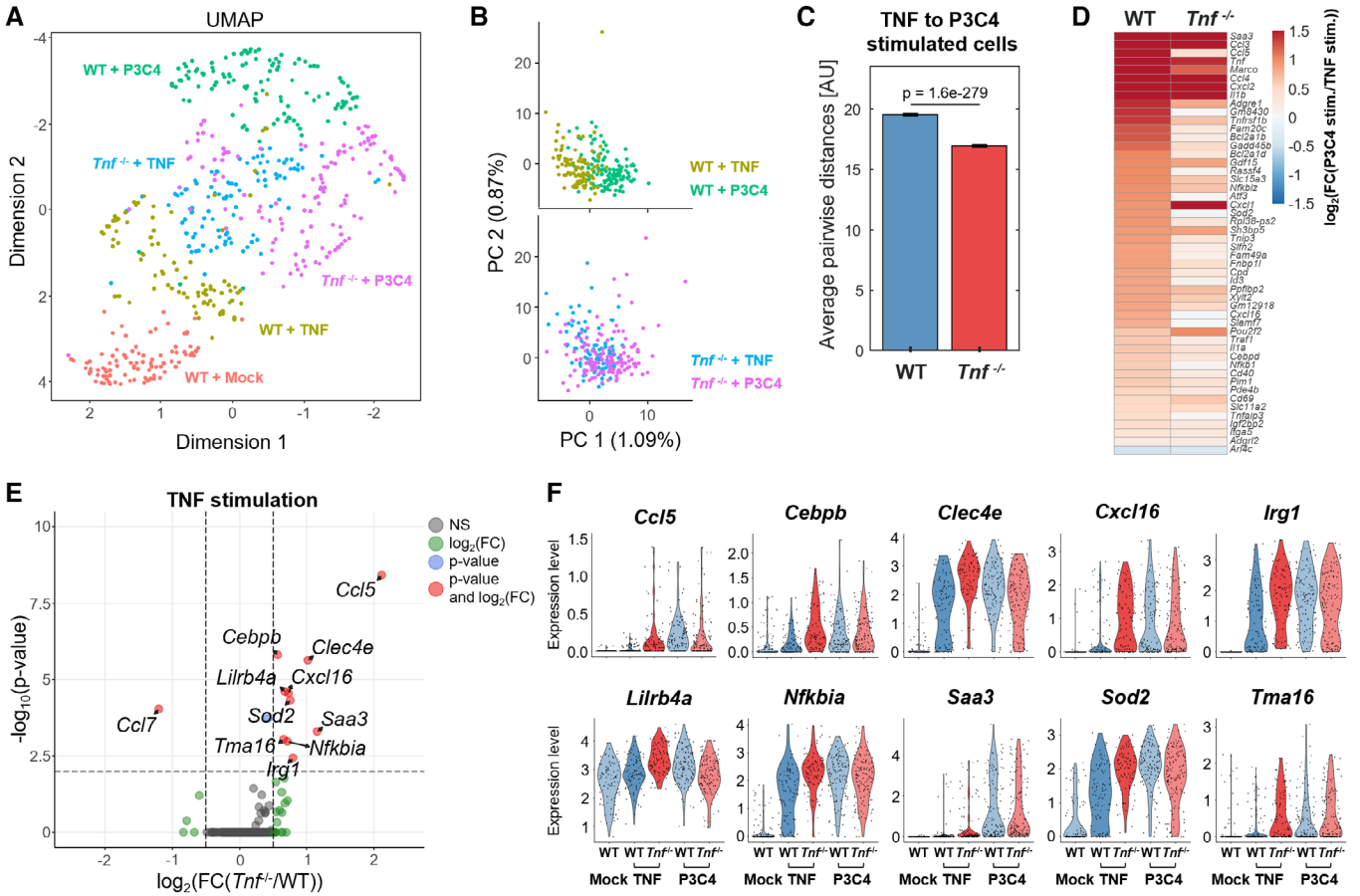

Figure 5. Tonic TNF conditioning controls TNF-induced gene expression.

A UMAP plot of single-cell gene expression in WT and *Tnf*$^{-/-}$ BMDMs stimulated with mock stimulation, 3.3 ng/ml TNF, or 10 ng/ml P3C4 for 4 h, measured by single-cell RNA-seq. Gene expression of 92 (WT mock), 95 (WT TNF), 123 (WT P3C4), 99 (*Tnf*$^{-/-}$ TNF), and 136 (*Tnf*$^{-/-}$ P3C4) cells was measured in one experiment.

B PCA plot of single-cell gene expression in WT (top) and *Tnf*$^{-/-}$ cells (bottom) upon TNF and P3C4 stimulation showing the first two PCA components.

C Average of all pairwise distances in the first 20 PCA components of single-cell gene expression between TNF and P3C4 stimulation in WT and *Tnf*$^{-/-}$ cells. Data are represented as mean of all pairwise distances ± SEM (WT: 123 × 95 = 11,685 distances; *Tnf*$^{-/-}$: 136 × 99 = 13,464 distances). Statistical significance was determined by Wilcoxon rank-sum test.

D Heatmap of $\log_2$(FC) between P3C4 versus TNF stimulation in WT and *Tnf*$^{-/-}$ cells for the top 50 (by *P*-value) genes differentially expressed in P3C4- versus TNF-stimulated WT cells.

E Volcano plot of single-cell gene expression in *Tnf*$^{-/-}$ versus WT BMDMs upon TNF stimulation. Dashed lines indicate *P*-value threshold of 0.01 and absolute $\log_2$(FC) threshold of 0.5. Only genes induced by P3C4 or TNF stimulation over mock in WT cells are included (*P*-value threshold of 0.05 and $\log_2$(FC) threshold of 0.25).

F Violin plots of single-cell gene expression in WT and *Tnf*$^{-/-}$ BMDMs upon mock, TNF, or P3C4 stimulation. The 10 genes shown are significantly upregulated in *Tnf*$^{-/-}$ versus WT cells upon TNF stimulation (see (E)).

expression of one (*Ccl7*) was decreased (Fig 5E). This, together with the asymmetry of the volcano plot toward positive fold-change values, indicated that, in the absence of tonic TNF, TNF-stimulated cells seem to hyper-respond to overlap with P3C4-stimulated cells. This interpretation was supported by examining the individual genes with significantly higher TNF-induced expression in *Tnf*$^{-/-}$ cells: *Ccl5*, *Cebpb*, *Clec4e*, *Cxcl16*, *Irg1*, *Lilrb4a*, *Nfkbia*, *Saa3*, *Sod2*, and *Tma16*. The single-cell distributions showed that their TNF-induced expression was increased in *Tnf*$^{-/-}$ cells compared to WT cells to more closely resemble P3C4-induced gene expression (Fig 5F). The more subtle changes in P3C4-induced gene expression at 4 h in *Tnf* $^{-/-}$ compared to WT BMDMs (Fig 5B and F) may result from the decreased duration of signaling (Fig 1H and I), presumably due to lack of autocrine TNF signaling (Caldwell *et al*, 2014).

Next, we investigated the effect of tonic TNF conditioning on another important function of stimulus-induced NFκB: the ability to alter the epigenome through formation of *de novo* enhancers which affects transcriptional responses to subsequent stimulations. Our previous work demonstrated that non-oscillatory NFκB has much greater capacity to form *de novo* enhancers than oscillatory NFκB (Cheng *et al*, 2021). We therefore hypothesized that tonic TNF may restrict the formation of *de novo* enhancers. H3K4me1 ChIP-seq analysis of WT and *Tnf* $^{-/-}$ BMDMs stimulated for 8 h with TNF, P3C4, or LPS revealed 1,515 peaks inducible by any stimulus compared to no stimulation (Fig 6A). Unsupervised k-means clustering resulted in a cluster of peaks appearing more weakly induced by TNF than P3C4 stimulation in WT cells, but more strongly induced by TNF in *Tnf* $^{-/-}$ cells compared to WT cells (Cluster 1); a cluster

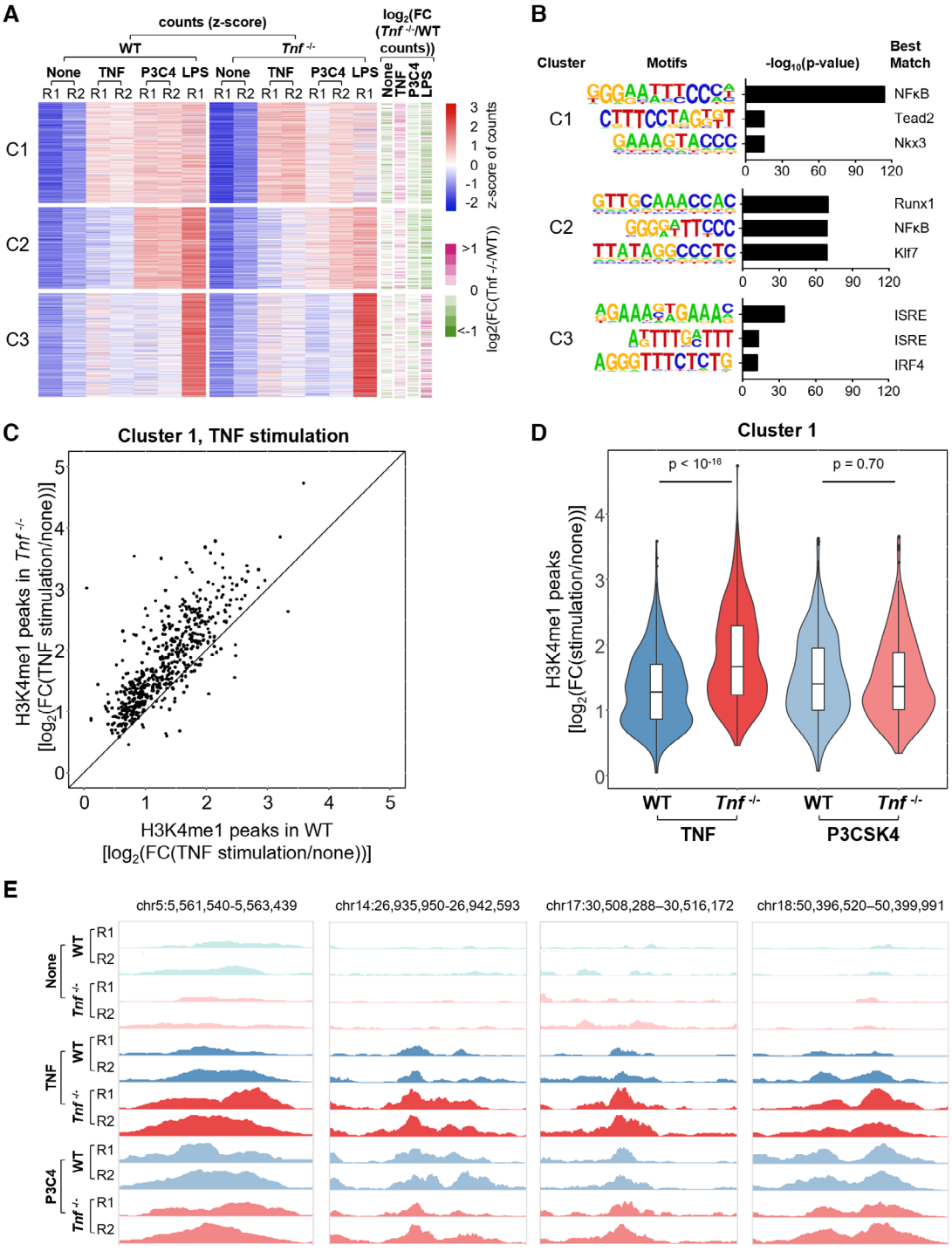

Figure 6.

very weakly induced by TNF stimulation in WT and *Tnf* $^{-/-}$ cells, well induced by P3C4 and LPS in WT cells, and less induced in *Tnf* $^{-/-}$ cells (Cluster 2); and a cluster of peaks strongly induced by LPS signaling, but not or weakly induced by other stimulations (Cluster 3; Fig 6A). Cluster 1 genomic regions were strongly enriched for NFκB-binding motifs, while Cluster 2 regions were enriched for Runx1-, NFκB-, and Klf7-binding motifs, and Cluster 3 regions were enriched for ISRE and IRF family-binding motifs (Fig 6B). Further analysis focused on Cluster 1 due to the prevalent NFκB-binding motifs suggesting NFκB-dependent enhancer formation. In Cluster 1, the fold change of H3K4me1 ChIP-seq signal induced by TNF over mock at many genomic regions was larger in *Tnf*$^{-/-}$ BMDMs than in WT BMDMs (Fig 6C). The distribution of fold changes of TNF-induced H3K4me1 ChIP-seq peak signals was significantly different in the absence of tonic TNF, while the P3C4-induced H3K4me1 ChIP-seq signal was not significantly altered (Fig 6D). Genome

Figure 6. Tonic TNF conditioning controls TNF-induced *de novo* enhancer formation.

A Heatmap of normalized H3K4me1 ChIP-seq counts in 1,515 inducible peaks in WT and $Tnf^{-/-}$ BMDMs unstimulated or stimulated with 10 ng/ml TNF, 100 ng/ml P3C4, or 100 ng/ml LPS for 8 h and heatmap of $\log_2$(FC) ($Tnf^{-/-}$ over WT) of mean H3K4me1 ChIP-seq counts. Unsupervised k-means clustering results in three clusters (C1-C3). One (for LPS) or two biological replicates (R1, R2) are shown.

B Top three hits from *de novo* motif analysis of regions in clusters C1-C3.

C Scatter plot of $\log_2$(FC) (TNF stimulated over unstimulated) of normalized H3K4me1 ChIP-seq signal in $Tnf^{-/-}$ BMDMs versus WT BMDMs within Cluster 1 regions (533 regions). Data are represented as mean of two biological replicates for each genomic region.

D Violin plot of $\log_2$(FC) of normalized H3K4me1 ChIP-seq signal in TNF- or P3C4-stimulated over unstimulated WT or $Tnf^{-/-}$ BMDMs within Cluster 1 regions (533 regions). Statistical significance was determined by Kolmogorov–Smirnov test. Data are represented as mean of two biological replicates for each genomic region. In the boxplot, central band indicates the median, boxes the interquartile range (IQR), and whiskers values within 1.5 IQR from the median.

E Examples of genomic regions with differential H3K4me1 signal in TNF stimulation in Cluster 1. Tracks for WT and $Tnf^{-/-}$ BMDMs unstimulated or stimulated with TNF or P3C4 in two biological replicates (R1, R2) are shown.

Data information: FC: fold change.

tracks of example genomic regions from Cluster 1 demonstrate the stronger induction of H3K4me1 ChIP-seq signal in TNF-treated $Tnf^{-/-}$ cells to levels matching or exceeding P3C4-induced peaks (Fig 6E). Thus, $Tnf^{-/-}$ cells were more likely to form TNF-induced *de novo* enhancers, especially in genomic regions with NFκB-binding motifs. In summary, the absence of tonic TNF conditioning increases both TNF-induced expression of NFκB response genes and formation of a set of NFκB motif-containing *de novo* enhancers.

Discussion

Here, we showed that macrophage conditioning by tonic, physiological levels of TNF safeguards the specificity of gene expression and epigenomic integrity in response to acute TNF exposure, ensuring that the responses to this host cytokine are distinct from PAMP-induced PRR signaling. We demonstrated that tonic TNF safeguards the oscillations in TNF-induced NFκB responses—which are key to the TNF's specific cellular responses—by decreasing TNFR signaling strength such that IKK activity does not neutralize the IκBα feedback loop.

The evidence for these findings comes from a variety of single-cell, biochemical, and genome-wide profiling assays. It is remarkable that subtle differences in the strength of signaling along the TNFR-IKK-NFκB axis, which established biochemical assays often fail to quantify with statistical significance, result in unmistakable differences in the temporal dynamics of NFκB revealed by live cell microscopy and substantial dysregulation of the functional effects of NFκB-driven gene expression and enhancer formation. This is a testament not only to the coarseness of biochemical assays compared to single-cell temporal trajectory data but also to the regulatory logic of the NFκB signaling pathway, where the IκBα-negative feedback loop sensitively interprets small differences in second-phase IKK activity levels to generate big differences in second-phase NFκB activity (Werner *et al*, 2005; Cheong *et al*, 2006; Adelaja *et al*, 2021). To substantiate the evidence for this mechanistic insight, we provided analyses based on computational simulation with an experimentally validated mathematical model of the NFκB signaling network (Fig 3) and a functional test via a genetic suppression strategy (Fig 4).

How then does tonic TNF conditioning modulate the TNFR-NFκB signaling axis? TNFR1 is known to be subject to complex regulation, including transcriptional and translational synthesis, trafficking to the cell surface from the Golgi TNFR1 pool, clustering into multimeric receptor units, ligand-induced oligomerization, endocytosis, recycling, and degradation, and TACE-dependent shedding, in addition to initiating signaling via recruitment of intracellular adaptors and signaling mediators TRAF2, TRADD, and RIPK. (Chan *et al*, 2000; Chan, 2007; Puimège *et al*, 2014; Kalliolias & Ivashkiv, 2016; Karathanasis *et al*, 2020). Since TNF-TNFR binding induces endocytosis of TNFR, we considered whether tonic TNF mildly increases the ligand-induced internalization rate of TNFR, slightly decreasing TNFR levels at baseline. Indeed, we found TNFR1 receptor surface levels elevated in $Tnf^{-/-}$ cells at baseline and after TNF-stimulated internalization (Figs 3E and EV3F). Interestingly, pre-incubation of the macrophage culture with low-dose exogenous TNF for 4 days did not fully rescue TNF-induced NFκB oscillations and thus does not mimic the full physiological effect of tonic TNF signaling (Fig EV1A–C). This suggests that mechanisms beyond short-term ligand-binding induced receptor internalization contribute to the difference in TNFR levels and IKK activity in WT and $Tnf^{-/-}$ macrophages. For example, TNF is synthesized as a transmembrane monomer, pro-TNF, which, upon transport to the cell membrane, trimerizes to form functional transmembrane TNF (tmTNF). An extracellular portion of the trimer is cleaved by the ADAM17/TACE protease and released as soluble TNF (sTNF; Kalliolias & Ivashkiv, 2016). Given the complexity of TNFR regulation, it is conceivable that tmTNF on neighboring cells or even intracellular or cell surface pro-TNF may play a role in TNFR regulation, rather than sTNF. Co-culture of $Tnf^{-/-}$ cells with WT cells, which might provide both sTNF and tmTNF via intercellular contacts, also did not rescue TNF-induced NFκB oscillations in $Tnf^{-/-}$ cells (Fig EV1D–F). This suggests a cell-intrinsic or autocrine mechanism and/or mechanisms acting earlier in macrophage differentiation or precursor development. Mathematical modeling revealed that even subtle effects on multiple TNFR-proximal biochemical reactions affecting TNFR surface levels and TNFR signaling functions may combine to mediate the observed reduction in oscillatory content in NFκB dynamics.

In immune sentinel cells, gene expression in response to PRR and cytokine signaling is stimulus specific, with the NFκB temporal code contributing much to that specificity (Hoffmann *et al*, 2002; Werner *et al*, 2005; Lane *et al*, 2017; Sheu *et al*, 2019; Adelaja *et al*, 2021). Decreased stimulus specificity in NFκB signaling and single-cell gene expression in a mouse model of the autoimmune disease Sjögren's syndrome underscores the importance of intact temporal coding for the maintenance of immune homeostasis (Adelaja *et al*, 2021). A key feature of this code is the distinction

between oscillatory NFκB dynamics elicited by the cytokine TNF and the non-oscillatory dynamics elicited by PAMPs. This study reveals a key determinant of the oscillatory content of NFκB dynamics in response to TNF stimulation, namely tonic TNF conditioning. Indeed, we show here that tonic TNF conditioning contributes to the specificity of TNF-induced gene expression. In the presence of tonic TNF, P3C4- and TNF-induced gene expression are distinguishable, but in its absence, they become more similar with TNF-induced expression of a subset of genes becoming more P3C4 like (Fig 5). The altered temporal code in *Tnf* $^{-/-}$ macrophages also leads to aberrant TNF-induced epigenetic reprogramming, particularly in genomic regions with NFκB-binding sites (Fig 6). Thus, conditioning by tonic TNF is essential for stimulus-appropriate NFκB signaling, immune gene responses, and the maintenance of epigenomic integrity.

As we show here, tonic TNF conditioning has profound effects on NFκB dynamics in cultured primary macrophages. *In vivo*, the levels of tonic TNF might be higher in a location-dependent manner due to the presence of microbiome PAMPs and DAMPs released during tissue turnover and repair. Consequently, tonic TNF conditioning may play a significant physiological role. Similarly, studies of interferons revealed the role of tonic cytokine signaling in fine tuning response set points. While abnormally high tonic IFN levels contribute to autoimmune diseases, decreased tonic signaling can be similarly detrimental to correct immune cell development and function, antiviral defense, and effective prevention of malignancies (Gough *et al*, 2012; Bradley *et al*, 2019; Marié *et al*, 2021). The results presented here may have implications for immunomodulation therapy with TNF inhibitors, which are a common treatment for chronic inflammatory conditions. While they are used as long-term therapeutics for, for example, rheumatoid arthritis, Crohn's disease, and psoriasis, their use may result in "paradoxical adverse events" (PAEs), that is, an exacerbation or new onset of inflammatory symptoms. The mechanisms mediating PAEs have not been fully elucidated, but are hypothesized to involve dysbalanced cytokine expression and subsequent misregulation of immune cells (Wendling & Prati, 2014; Toussirot & Aubin, 2016). Whether subtle changes in TNFR dynamics elicited by reduced tonic TNF conditioning and loss of oscillatory content in NFκB with resulting loss of epigenomic integrity are relevant mechanistic explanations for this pathological condition may be the subject of future studies.

Materials and Methods

Macrophage cell culture, stimulation, and RNA interference

Mice were housed and handled according to guidelines established by the UCLA Animal Research Committee under an approved protocol. UCLA's current Animal Welfare Assurance identification number is D16-00124 (A3196-01). Macrophages were produced from wild-type C57BL/6 mice (JAX strain 000664), mVenus-RelA (*Rela*$^{V/V}$) mice (Adelaja *et al*, 2021), *Tnf*$^{-/-}$ mice (JAX strain 005540), and p100$^{-/-}$ mice. The latter express p52 protein from the *Nfkb2* gene, as they were generated by a CRISPR frameshift mutation at amino acid L462 in the linker region prior to the ankyrin repeat domain of *Nfkb2*. Bone marrow was isolated from murine tibias and femurs from male and female 6- to 14-week-old mice followed by red blood cell lysis. BMDMs were differentiated in IMDM media (Gibco 12440061) supplemented with 10% ES cell FBS (Gibco 10439024), 100 IU penicillin, 100 μg/ml streptomycin, 2 mM L-glutamine, 55 μM 2-mercaptoethanol, and 30% L929-cell supernatant in 15 cm TC-treated dishes. On Day 4, cells were detached using a cell lifter and replated into experimental culture plates, unless otherwise indicated. Cells were stimulated on Day 7 or 8 at the indicated concentrations with recombinant mouse TNF-alpha (aa 80–235) protein (410-MT-010, R&D Systems), Pam3CSK4 (tlrl-pms, Invivogen), or LPS (L6529-1MG, Sigma-Aldrich) for the indicated time. For stimulation, one-fifth of the conditioned cell culture media were removed, mixed with stimulus, and added to the cells at the time of stimulation. For culture of BMDMs in the presence of low-dose TNF, the BMDM media were supplemented with 250 pg/ml TNF starting at time of replating on Day 4. Media were changed every 24 h to replenish TNF. As a control, media on cells incubated without low-dose TNF were also changed every 24 h. For co-culture experiments, 15% *Tnf* $^{-/-}$ *Rela*$^{V/V}$ BMDMs were plated with 85% WT *Rela*$^{+/+}$ BMDMs (i.e., non-fluorescent) at the time of replating on Day 4. For experiments with siRNA-mediated reduction in TNFR1 expression, cells were transfected with 20 nM non-targeting control siRNA pool (horizon D-001810-10-05) or 2 nM TNFR1 siRNA pool (horizon L-060201-01-0005) + 18 nM control siRNA using 2.5 μl/ml Lipofectamine RNAiMax (Invitrogen 13778075) according to the manufacturer's instructions 24 h before the experiment.

Live-cell fluorescence microscopy

For measurement of nuclear NFκB dynamics, BMDMs were replated on Day 4 at a density of 15,000–35,000 cells/cm^2 in 400 μl media in an eight-well μ-Slide (ibidi). On day 7 or 8, cells were subjected to live cell imaging using a previously established workflow (Adelaja *et al*, 2021). Before imaging, 6.25 ng/ml Hoechst 33342 was added to the cells, and cells were placed on an Axio Observer.Z1 inverted microscope (Zeiss) with live-cell incubation for at least 90 min to equilibrate to environmental conditions. Using automated image acquisition in Zen 2.3 software, at least five positions per condition (maximum eight conditions per experiment) were imaged at one frame per 5 min using a Plan-Apochromat 20×/0.8 NA M27 air objective. Images were collected sequentially in three channels, for mVenus fluorescence (filter set: Zeiss 46 HE, ex.: 500/25 nm, beam splitter: 515 nm, em.: 535/30 nm; Colibri.2 505 nm, 90% power; exposure: 160 ms), Hoechst fluorescence (filter set: Zeiss 49, ex.: 365 nm, beam splitter: 395 nm, em.: 445/50 nm; X-Cite 120; exposure: 50 ms), and differential interference contrast (DIC; HAL 100 lamp; 2.3 V, exposure: 20 ms). Images were recorded on a Hamamatsu Orca Flash4.0 CMOS camera with 2 × 2 binning. After collection of baseline image(s), the indicated stimulus diluted in conditioned media was applied using syringe injection into the chamber *in situ* and images were acquired for 8 or 11.5 h.

Automated image analysis and feature calculations

Individual channel images were exported in Zen lite 3.3 software. Single cells were segmented into cytoplasm and nucleus, tracked across the time course, and mVenus-RelA nuclear fluorescence was quantified using MACKtrack (https://github.com/signalingsystemslab/

MACKtrack) in MATLAB as described previously (Adelaja *et al*, 2021). Dynamic features of single-cell NFκB trajectories were calculated using code available here: https://github.com/signalingsystemslab/nfkb_dynamic_features. The percentage of oscillating cells was calculated from the frequency feature using a cutoff of 0.42 h^{-1}. To determine nuclear mVenus-RelA fluorescence levels in unstimulated WT and $Tnf^{-/-}$ BMDMs, the mean fluorescence values after background adjustment over 60 min were used. For the co-culture experiments, only NFκB trajectories with a maximum amplitude of >2.6 were included in the analysis to avoid erroneous inclusion of WT ($Rela^{+/+}$) cells that had taken up $Tnf^{-/-}$ $Rela^{V/V}$ cells by phagocytosis.

ELISA

For measurement of tonic TNF and stimulation-induced TNF secretion, BMDMs were replated on Day 4 at a density of 22,000/cm^2 in 2.5 ml media in a six-well format. On Day 7 or 8, cells were stimulated as indicated. At harvest time points, cell culture supernatants were frozen at −80°C. TNF concentrations in supernatants were determined by mouse TNF-alpha DuoSet ELISA (DY410-05) according to the manufacturer's instructions.

RT–qPCR

For determination of Iκbα mRNA levels, BMDMs were replated on Day 4 at a density of 22,000/cm^2 in a six-well format. On Day 7 or 8, cells were stimulated as indicated. At harvest time points, cells were placed on ice and lysed with 350 µl TRIzol reagent. Total RNA was purified using Direct-zol RNA miniprep kit (Zymo Research). cDNA was generated using iScript™ Reverse Transcription Supermix (Bio-Rad) or LunaScript® RT SuperMix Kit (NEB). qPCR was performed on the CFX384 Real-Time system (Bio-Rad) using the SsoAdvanced Universal SYBR® Green Supermix (Bio-Rad) with the following primer pairs: Iκbα: 5′- AGACTCGTTCCTGCACTTG, 5′- AGTCTGCTGCAGGTTGTTC; GAPDH: 5′- AATGGTGAAGGTCGG TGTG, 5′- GTGGAGTCATACTGGAACATGTAG.

Western blotting

For determination of protein levels in whole-cell lysates, BMDMs were replated on Day 4 at a density of 22,000/cm^2 in a six-well format. On Day 7 or 8, cells were stimulated as indicated. At harvest time points, cells were placed on ice, washed in the plate with cold PBS, lysed directly with β-mercaptoethanol-containing Laemmli sample buffer (Bio-Rad), and incubated at 95°C for 5 min. Proteins were separated by SDS–PAGE (Criterion TGX 4–5% gel, Bio-Rad) and transferred to PVDF membranes using wet transfer. Blocking of membranes was carried out in 5% bovine serum albumin (BSA) for 1 h at room temperature (RT), followed by incubation with primary antibodies at 4°C for 16 h. Membranes were incubated with appropriate HRP-conjugated secondary antibodies (Cell Signaling Technology) for 1 h at RT and developed using Super Signal West Femto and Super Signal West Pico Plus chemiluminescent substrate (Thermo Scientific). The following primary antibodies were used: α-A20 (sc-166692, 1:1,000), α-IKKβ (CST2678, 1:1,000), α-phospho-IKK (Ser176/180; CST2697, 1:1,000), α-phospho-JNK (Thr183/Tyr185; CST4668, 1:1,000), α-phospho-ERK (Thr202/Tyr204; CST4370, 1:1,000), α-phospho-p38 (Thr180/Tyr182; CST4511, 1:3,000), and α-tubulin (T5201, Sigma-Aldrich, 1:5,000). Protein levels were quantified by measuring mean gray value using ImageJ, deducting background value per lane, and dividing by background-corrected β-tubulin bands.

Electrophoretic mobility shift assay (EMSA)

For determination of nuclear NFκB activity, BMDMs were replated on Day 4 at a density of 19,000/cm^2 in a 10 cm dish. On Day 7, cells were stimulated as indicated. At harvest time point, cells were washed with cold PBS and lysed in 100 µl cytosolic extract buffer (10 mM HEPES pH 7.9, 10 mM KCl, 0.1 mM EGTA, 0.1 mM EDTA, freshly supplemented with 1 mM DTT, 0.5 mM PMSF, 4 µg/ml leupeptin, 1 µM pepstatin A, 0.01 TIU/ml aprotinin, and 1:100 phosphatase inhibitor cocktail I + II [Calbiochem]). Cells were scraped, transferred to microcentrifuge tubes, and incubated on ice for 5 min. NP-40 was added to a final concentration of 0.2%, followed by a 30 s incubation, 30 s vortexing, and 40 s centrifugation at 12,000 *g*. After removal of the supernatant, the nuclei were incubated in 10 µl nuclear extract buffer (20 mM HEPES pH 7.9, 420 mM NaCl, 1.5 mM MgCl, 0.2 mM EDTA, and 25% glycerol, supplemented as above) for 10 min, with 5 s vortexing every 2 min. Nuclear extracts were cleared of debris by centrifugation at 16,000 *g* for 5 min at 4°C. EMSA was performed as described previously (Hoffmann *et al*, 2002; Ngo *et al*, 2020). 2.5 µl of nuclear extract were incubated with 0.013 pmole ^{32}P-labeled double-stranded oligonucleotide probe in 2× binding buffer (10 mM Tris–HCl pH7.5, 50 mM NaCl, 10% glycerol, 1% NP-40, 1 mM EDTA, and 0.1 mg/ml poly-dIdC) for 10 min. The following probes were used: 5′-GCTACAAGGGACTTTCCG CTGGGGACTTTCCAGGGAGG-3′, 5′-CCTCCCTGGAAAGTCCCCAGC GGAAAGTCCCTT GTAGC-3′ containing two consensus κB sites for NFκB binding; 5′-GATTTTTTCCTGATTGGTTAAA-3′; 5′-ACTTTTAA CCAATCAGGAAAAA-3′ for NF-Y binding as a normalization control. DNA–protein complexes were resolved on a non-denaturing 5% acrylamide (30:0.8) gel at 200 V for 1:45 h. The gel was dried and used to expose a storage phosphor screen. The signal was measured using an Amersham Typhoon Imager (GE Healthcare). NFκB bands were quantified by measuring mean gray value using ImageJ, deducting background value per lane, and dividing by background-corrected NF-Y bands.

Flow cytometry

To measure cell surface expression of CD120a (TNFR1), CD120b (TNFR2), and CD11b, BMDMs were replated on Day 4 at a density of 22,000/cm^2 in a six-well format. On Day 7, cells were stimulated as indicated. At harvest time point, cells were placed on ice, washed in the plate with cold PBS, harvested by gentle scraping in cold PBS, and passed through a 40 µm cell strainer. After Fc blocking for 15 min using α-CD16/32 antibody (BioLegend 101301, 1:50), each sample was split to be incubated with APC α-CD11b (BioLegend 101212, 1:333), APC-α-CD120a (BioLegend 113005, 1:100), or biotin α-CD120b (BioLegend 113403, 1:100) for 45 min. The α-CD120b-stained sample was further incubated with APC-Strepavidin (BioLegend 405207, 1:500) for 10 min. 7AAD (BioLegend 420404, 1:100) was added as a viability dye. Flow cytometry was performed on CytoFLEX flow cytometer (Beckman Coulter). Data were analyzed using FlowJo v10. Median fluorescence intensity (MFI) of unstained

control was deducted from MFI of stained samples before calculation of relative expression levels. For measuring cell surface expression of CD120a after TNFR1 siRNA transfection, cells were replated on Day 4 in a 12-well format, transfected with siRNA 24 h before the experiment, and analyzed using α-CD120a antibody as above.

Single-cell RNA-seq by Fluidigm

For single-cell gene expression measurements, app. 300,000 BMDMs were plated in 6 cm dishes. On Day 7, cells were stimulated as indicated. After 4 h, cells were washed with PBS, detached using Accutase, and placed on ice at a density of app. 350,000 cells/ml in PBS. Then, the Fluidigm C1 system was used for single-cell RNA-seq using 3 mRNA HT IFCs. Paired-end 2×100 reads were collected on an Illumina HiSeq at the Broad Stem Cell Research Center sequencing core at UCLA. Reads were quality filtered and adapter trimmed with cutadapt (Martin, 2011). Demultiplexing was performed using the Fluidigm C1 mRNA HT demultiplexer Perl script. Ribosomal reads were removed from read 2 FASTQ files by alignment with bowtie2 (Langmead & Salzberg, 2012). Gene-level counts were obtained using RSEM with an mm10 reference (Li & Dewey, 2011). QC was performed using SinQC (Jiang *et al*, 2016). Gene symbols were assigned to gene IDs using biomaRt (Durinck *et al*, 2009). Cells were retained if all the following conditions were met: at least 100,000 mapped reads, a mapping rate of at least 0.6, library complexity of at least 0.4, number of detected genes between 2,000 and 4,300, and a fraction of mitochondrial reads $< 12\%$. This resulted in 545 high-quality cells retained. Seurat was used to log-normalize counts, regressing out sequencing depth (Hao *et al*, 2021). UMAP was performed using the uwot R package on the first 20 PCA components, with 20 neighbors, a learning rate of 0.1, and a scaled PCA initialization (Melville, 2022). Differential gene expression analysis was performed with Seurat (min log fold-change threshold of 0.1 and min percent difference of 0.05). Average of all pairwise distances between gene expression in TNF- and P3C4-stimulated cells was calculated by computing the Euclidean distance between cell values along the first 20 PCA components.

H3K4me1 ChIP-seq

For H3K4me1 ChIP-seq, BMDMs were replated on Day 4 at a density of 19,000/cm^2 in a 10 cm dish. On Day 7, cells were stimulated as indicated. After 8 h, BMDMs were cross-linked with 1% formaldehyde, quenched with 125 mM glycine, frozen, and stored at −80°C. Cell lysis, chromatin fragmentation, H3K4me1 immunoprecipitation using Abcam ab8895 antibody, RNAse treatment, crosslinking reversal, DNA fragment purification, sequencing library preparation, and Illumina sequencing at Technology Center for Genomics & Bioinformatics at UCLA were performed as described (Cheng *et al*, 2021). MACS2 version 2.1.0 was used in broad mode to identify peaks for each sample using pooled input samples as control, FDR < 0.01, and extension size of average fragment length (Zhang *et al*, 2008). These peaks were merged to generate a single reference peak file, and the number of reads in each peak was counted using deeptools multiBamSummary with extension size of average fragment length. edgeR was used to construct a negative binomial model, and inducible peaks were identified in any stimulation condition compared to unstimulated by FDR < 0.05 and $\log_2$FC > 1 (Robinson *et al*, 2010). Out of $> 89{,}000$ peaks, 1,515 were identified as *de novo*, stimulus-inducible peaks. Read counts were normalized to counts per million for each sample. Heatmaps were generated with the pheatmap R package. Analysis of transcription factor motif enrichment was performed using findMotifsGenome function in the HOMER suite, using the entire width of differential peaks as foreground and all detected peaks as background (Heinz *et al*, 2010).

Mathematical modeling

A well-established ordinary differential equations (ODE) model of NFκB signaling was used to investigate the mechanisms responsible for altered NFκB dynamics (Adelaja *et al*, 2021). The importance of 13 parameters within the TNF module in determining oscillations was analyzed by parameter scanning, increasing or decreasing default values by $10^{\pm 0.1}$ to $10^{\pm 1}$ times (10 values spaced logarithmically). Five parameters were found to control the oscillatory potential: increase k_{54}, decrease k_{61}, increase k_{62}, decrease k_{63}, and increase k_{65}. To model the heterogeneity of cells, a (joint) log-normal distribution of the chosen parameters (k_{54}, k_{61}, k_{62}, k_{63}, and k_{65}) was used with the variance specifying that 99% of the values locate within a twofold range. To model $Tnf^{-/-}$ cells, the means of parameter distributions were changed by $10^{\pm 0.1}$. Single and paired parameters were sampled. Oscillation power was calculated for each simulated single-cell trajectory using FFT in the frequency band 0.33 to 1 h^{-1}. Cells were categorized as oscillatory if they passed a threshold of 2×10^{-4} μM^2 h^{-1}. To investigate whether increasing NFκB abundance could rescue the oscillations in $Tnf^{-/-}$, the total amount of NFκB was changed from 0.08 μM to 0.1 μM (1.25×). A total of 2,000 cells and 1,000 cells were simulated for the "WT" versus "$Tnf^{-/-}$" comparison and "1× NFκB" versus "1.25× NFκB" comparison, respectively. The ODE model was solved in Matlab using ode15s. Simulations involved a first phase to establish steady state, and then a second phase of TNF stimulation. All the results are visualized in MATLAB.

Experimental design and statistical analysis

Unless otherwise indicated, biological replicates are reported, which were produced using independent BMDM preparations from different mice on different days. Experimental samples were blinded by using numbering codes for sample tubes by which the sample could be processed without awareness of its role in the experimental design. The limited availability and high cost of procuring samples determined the sample size for some experiments. Statistical tests were performed as described in the figure legends. In brief, differences in means and medians of read-outs were tested using *t*-tests or Wilcoxon rank-sum tests, respectively, as appropriate for the assumed underlying distribution shape and variance. Differences in distributions were compared using the Kolmogorov–Smirnov test.

Data availability

The code to perform the mathematical modeling simulations is available here: https://github.com/signalingsystemslab/TNFKO_NFkB_dynamics_modeling.

The code for MACKtrack for automated cell segmentation, tracking, and quantification is available here: https://github.com/signalingsystemslab/MACKtrack.

The code to calculate NFκB dynamics features is available here: https://github.com/signalingsystemslab/nfkb_dynamic_features.

The single-cell NFκB trajectories are available as Source Data.

The scRNA-seq and ChIP-Seq datasets produced in this study are available in the following databases:

- Single-cell RNA-seq by Fluidigm: Gene Expression Omnibus GSE209565 https://www.ncbi.nlm.nih.gov/geo/query/acc.cgi?acc=GSE209565.
- H3K4me1 ChIP-Seq: Gene Expression Omnibus GSE209565 https://www.ncbi.nlm.nih.gov/geo/query/acc.cgi?acc=GSE209565.

Other data are available upon request.

Expanded View for this article is available online.

Acknowledgements

We thank Kylie Farrell Satula for mouse breeding and colony maintenance and Emily Chen for technical assistance. S.L. was funded by the Deutsche Forschungsgemeinschaft (DFG, German Research Foundation)—419234150. A.A. was funded by NIH grants F31AI138450-01A1, T32GM008042, and T32HL069766; and A.S. was funded by NIH grant T32GM008185. The work was funded by NIH grants to A.H.—R01AI127864 and R01AI132731.

Author contributions

Stefanie Luecke: Conceptualization; formal analysis; investigation; visualization; methodology; writing – original draft. **Adewunmi Adelaja:** Conceptualization; software; formal analysis; investigation; methodology. **Xiaolu Guo:** Software; investigation; visualization; methodology. **Supriya Sen:** Investigation; methodology. **Roberto Spreafico:** Formal analysis; investigation; visualization; methodology. **Apeksha Singh:** Formal analysis; investigation; visualization. **Yi Liu:** Investigation; methodology. **Brooks Taylor:** Investigation; methodology. **Jessica Diaz:** Investigation; methodology. **Quen Cheng:** Formal analysis; supervision; investigation; visualization. **Alexander Hoffmann:** Conceptualization; resources; supervision; funding acquisition; project administration; writing – review and editing.

Disclosure and competing interests statement

The authors declare that they have no conflict of interest.

References

Adelaja A, Taylor B, Sheu KM, Liu Y, Luecke S, Hoffmann A (2021) Six distinct NFκB signaling codons convey discrete information to distinguish stimuli and enable appropriate macrophage responses. *Immunity* 54: 916–930.e7

Ando M, Magi S, Seki M, Suzuki Y, Kasukawa T, Lefaudeux D, Hoffmann A, Okada M (2021) IκBα is required for full transcriptional induction of some NFκB-regulated genes in response to TNF in MCF-7 cells. *NPJ Syst Biol Appl* 7: 1–15

Basak S, Kim H, Kearns JD, Tergaonkar V, O'Dea E, Werner SL, Benedict CA, Ware CF, Ghosh G, Verma IM *et al* (2007) A fourth IkappaB protein within the NF-kappaB signaling module. *Cell* 128: 369–381

Behar M, Hoffmann A (2013) Tunable signal processing through a kinase control cycle: the IKK signaling node. *Biophys J* 105: 231–241

Bradley KC, Finsterbusch K, Schnepf D, Crotta S, Llorian M, Davidson S, Fuchs SY, Staeheli P, Wack A (2019) Microbiota-driven tonic interferon signals in lung stromal cells protect from influenza virus infection. *Cell Rep* 28: 245–256.e4

Caldwell AB, Cheng Z, Vargas JD, Birnbaum HA, Hoffmann A (2014) Network dynamics determine the autocrine and paracrine signaling functions of TNF. *Genes Dev* 28: 2120–2133

Catrysse L, Vereecke L, Beyaert R, van Loo G (2014) A20 in inflammation and autoimmunity. *Trends Immunol* 35: 22–31

Chan FK-M (2007) Three is better than one: pre-ligand receptor assembly in the regulation of TNF receptor signaling. *Cytokine* 37: 101–107

Chan FK-M, Chun HJ, Zheng L, Siegel RM, Bui KL, Lenardo MJ (2000) A domain in TNF receptors that mediates ligand-independent receptor assembly and signaling. *Science* 288: 2351–2354

Cheng Z, Taylor B, Ourthiague DR, Hoffmann A (2015) Distinct single-cell signaling characteristics are conferred by the MyD88 and TRIF pathways during TLR4 activation. *Sci Signal* 8: ra69

Cheng CS, Behar MS, Suryawanshi GW, Feldman KE, Spreafico R, Hoffmann A (2017) Iterative modeling reveals evidence of sequential transcriptional control mechanisms. *Cell Syst* 4: 330–343.e5

Cheng QJ, Ohta S, Sheu KM, Spreafico R, Adelaja A, Taylor B, Hoffmann A (2021) NF-κB dynamics determine the stimulus specificity of epigenomic reprogramming in macrophages. *Science* 372: 1349–1353

Cheong R, Bergmann A, Werner SL, Regal J, Hoffmann A, Levchenko A (2006) Transient IκB kinase activity mediates temporal NF-κB dynamics in response to a wide range of tumor necrosis factor-α doses *. *J Biol Chem* 281: 2945–2950

Covert MW, Leung TH, Gaston JE, Baltimore D (2005) Achieving stability of lipopolysaccharide-induced NF-kappaB activation. *Science* 309: 1854–1857

Durinck S, Spellman PT, Birney E, Huber W (2009) Mapping identifiers for the integration of genomic datasets with the R/Bioconductor package biomaRt. *Nat Protoc* 4: 1184–1191

Gough DJ, Messina NL, Clarke CJP, Johnstone RW, Levy DE (2012) Constitutive type I interferon modulates homeostatic balance through tonic signaling. *Immunity* 36: 166–174

Hao Y, Hao S, Andersen-Nissen E, Mauck WM, Zheng S, Butler A, Lee MJ, Wilk AJ, Darby C, Zager M *et al* (2021) Integrated analysis of multimodal single-cell data. *Cell* 184: 3573–3587.e29

Heinz S, Benner C, Spann N, Bertolino E, Lin YC, Laslo P, Cheng JX, Murre C, Singh H, Glass CK (2010) Simple combinations of lineage-determining transcription factors prime cis-regulatory elements required for macrophage and B cell identities. *Mol Cell* 38: 576–589

Hoffmann A, Levchenko A, Scott ML, Baltimore D (2002) The IkappaB-NF-kappaB signaling module: temporal control and selective gene activation. *Science* 298: 1241–1245

Jiang P, Thomson JA, Stewart R (2016) Quality control of single-cell RNA-seq by SinQC. *Bioinformatics* 32: 2514–2516

Kalliolias GD, Ivashkiv LB (2016) TNF biology, pathogenic mechanisms and emerging therapeutic strategies. *Nat Rev Rheumatol* 12: 49–62

Karathanasis C, Medler J, Fricke F, Smith S, Malkusch S, Widera D, Fulda S, Wajant H, van Wijk SJL, Dikic I *et al* (2020) Single-molecule imaging reveals the oligomeric state of functional TNFα-induced plasma membrane TNFR1 clusters in cells. *Sci Signal* 13: eaax5647

Lane K, Van Valen D, DeFelice MM, Macklin DN, Kudo T, Jaimovich A, Carr A, Meyer T, Pe'er D, Boutet SC *et al* (2017) Measuring signaling and RNA-Seq in the same cell links gene expression to dynamic patterns of NF-kappaB activation. *Cell Syst* 4: 458–469.e5

Langmead B, Salzberg SL (2012) Fast gapped-read alignment with bowtie 2. *Nat Methods* 9: 357–359

Lee REC, Walker SR, Savery K, Frank DA, Gaudet S (2014) Fold change of nuclear NF-κB determines TNF-induced transcription in single cells. *Mol Cell* 53: 867–879

Li B, Dewey CN (2011) RSEM: accurate transcript quantification from RNA-Seq data with or without a reference genome. *BMC Bioinformatics* 12: 323

Marié IJ, Brambilla L, Azzouz D, Chen Z, Baracho GV, Arnett A, Li HS, Liu W, Cimmino L, Chattopadhyay P *et al* (2021) Tonic interferon restricts pathogenic IL-17-driven inflammatory disease via balancing the microbiome. *Elife* 10: e68371

Martin M (2011) Cutadapt removes adapter sequences from high-throughput sequencing reads. *EMBnetJ* 17: 10–12

McDermott MF, Aksentijevich I, Galon J, McDermott EM, Ogunkolade BW, Centola M, Mansfield E, Gadina M, Karenko L, Pettersson T *et al* (1999) Germline mutations in the extracellular domains of the 55 kDa TNF receptor, TNFR1, define a family of dominantly inherited autoinflammatory syndromes. *Cell* 97: 133–144

Melville J (2022) uwot: the Uniform Manifold Approximation and Projection (UMAP) method for dimensionality reduction. R package version 0.1.14. https://CRAN.R-project.org/package=uwot

Mitchell S, Vargas J, Hoffmann A (2016) Signaling via the NFκB system. *Wiley Interdiscip Rev Syst Biol Med* 8: 227–241

Murray PJ, Wynn TA (2011) Protective and pathogenic functions of macrophage subsets. *Nat Rev Immunol* 11: 723–737

Ngo KA, Kishimoto K, Davis-Turak J, Pimplaskar A, Cheng Z, Spreafico R, Chen EY, Tam A, Ghosh G, Mitchell S *et al* (2020) Dissecting the regulatory strategies of NF-κB RelA target genes in the inflammatory response reveals differential transactivation logics. *Cell Rep* 30: 2758–2775.e6

Pękalski J, Zuk PJ, Kochańczyk M, Junkin M, Kellogg R, Tay S, Lipniacki T (2013) Spontaneous NF-κB activation by autocrine TNFα signaling: a computational analysis. *PLoS ONE* 8: e78887

Puimège L, Libert C, Van Hauwermeiren F (2014) Regulation and dysregulation of tumor necrosis factor receptor-1. *Cytokine Growth Factor Rev* 25: 285–300

Robinson MD, McCarthy DJ, Smyth GK (2010) edgeR: a Bioconductor package for differential expression analysis of digital gene expression data. *Bioinformatics* 26: 139–140

Rouillard AD, Gundersen GW, Fernandez NF, Wang Z, Monteiro CD, McDermott MG, Ma'ayan A (2016) The harmonizome: a collection of processed datasets gathered to serve and mine knowledge about genes and proteins. *Database* 2016: baw100

Savinova OV, Hoffmann A, Ghosh G (2009) The Nfkb1 and Nfkb2 proteins p105 and p100 function as the core of high-molecular-weight heterogeneous complexes. *Mol Cell* 34: 591–602

Schütze S, Tchikov V, Schneider-Brachert W (2008) Regulation of TNFR1 and CD95 signalling by receptor compartmentalization. *Nat Rev Mol Cell Biol* 9: 655–662

Sedger LM, McDermott MF (2014) TNF and TNF-receptors: from mediators of cell death and inflammation to therapeutic giants – past, present and future. *Cytokine Growth Factor Rev* 25: 453–472

Sen S, Cheng Z, Sheu KM, Chen YH, Hoffmann A (2020) Gene regulatory strategies that decode the duration of NFκB dynamics contribute to LPS- versus TNF-specific gene expression. *Cell Syst* 10: 169–182.e5

Sheu KM, Luecke S, Hoffmann A (2019) Stimulus-specificity in the responses of immune sentinel cells. *Curr Opin Syst Biol* 18: 53–61

Shih VF-S, Kearns JD, Basak S, Savinova OV, Ghosh G, Hoffmann A (2009) Kinetic control of negative feedback regulators of NF-kappaB/RelA determines their pathogen- and cytokine-receptor signaling specificity. *Proc Natl Acad Sci USA* 106: 9619–9624

Toussirot É, Aubin F (2016) Paradoxical reactions under TNF-α blocking agents and other biological agents given for chronic immune-mediated diseases: an analytical and comprehensive overview. *RMD Open* 2: e000239

Wendling D, Prati C (2014) Paradoxical effects of anti-TNF-α agents in inflammatory diseases. *Expert Rev Clin Immunol* 10: 159–169

Werner SL, Barken D, Hoffmann A (2005) Stimulus specificity of gene expression programs determined by temporal control of IKK activity. *Science* 309: 1857–1861

Werner SL, Kearns JD, Zadorozhnaya V, Lynch C, O'Dea E, Boldin MP, Ma A, Baltimore D, Hoffmann A (2008) Encoding NF-kappaB temporal control in response to TNF: distinct roles for the negative regulators IkappaBalpha and A20. *Genes Dev* 22: 2093–2101

Wertz IE, O'Rourke KM, Zhou H, Eby M, Aravind L, Seshagiri S, Wu P, Wiesmann C, Baker R, Boone DL *et al* (2004) De-ubiquitination and ubiquitin ligase domains of A20 downregulate NF-κB signalling. *Nature* 430: 694–699

Wu R, Kang R, Tang D (2022) Mitochondrial ACOD1/IRG1 in infection and sterile inflammation. *J Intensive Med* 2: 78–88

Yılmaz ZB, Kofahl B, Beaudette P, Baum K, Ipenberg I, Weih F, Wolf J, Dittmar G, Scheidereit C (2014) Quantitative dissection and modeling of the NF-κB p100-p105 module reveals interdependent precursor proteolysis. *Cell Rep* 9: 1756–1769

Zhang Y, Liu T, Meyer CA, Eeckhoute J, Johnson DS, Bernstein BE, Nusbaum C, Myers RM, Brown M, Li W *et al* (2008) Model-based analysis of ChIP-Seq (MACS). *Genome Biol* 9: R137

Expanded View Figures

Figure EV1. Supplementation of *Tnf*$^{-/-}$ BMDMs culture media with low-dose TNF only partially restores TNF-induced NFκB oscillations and co-culture with WT BMDMs does not.

A–F Nuclear localization of mVenus-RelA upon stimulation with 10 ng/ml TNF was measured over time by fluorescence microscopy in *Tnf*$^{-/-}$ *Rela*$^{V/V}$ BMDMs cultured for 4 days in the absence or presence of 250 pg/ml TNF ("preTNF") (A-C) or 85% WT (*Rela*$^{+/+}$) (non-fluorescent) cells (D–F). Nuclear mVenus-RelA was quantified by automated image analysis. (A, D) Each row of the heatmap represents the NFκB signaling trajectory of one cell. Trajectories are sorted by maximum amplitude. Example trajectories are shown below. Data from a single representative experiment are depicted. (B, E) Indicated dynamic features were calculated from signaling trajectories. Violin plots depict pooled data from three biological replicates (total # of cells: 2,211/1,791) (B) or six biological replicates (total # of cells: 12,059/1,889) (E). Marker indicates median of distribution. Statistical significance was determined by Wilcoxon rank-sum test. Number indicates $\log_{10}$(*P*-value). (C, F) Percentage of cells with NFκB trajectories categorized as oscillatory based on a frequency threshold among all responder cells in each experiment. Data are represented as mean ± SD of three (C) or six (F) biological replicates. Statistical significance was determined by one-tailed paired-sample *t*-test. (D–F) For the co-culture experiment, only NFκB trajectories with a max amplitude of > 2.6 were included in the analysis to avoid erroneous inclusion of WT (*Rela*$^{+/+}$) cells that had taken up *Tnf*$^{-/-}$ *Rela*$^{V/V}$ cells by phagocytosis.

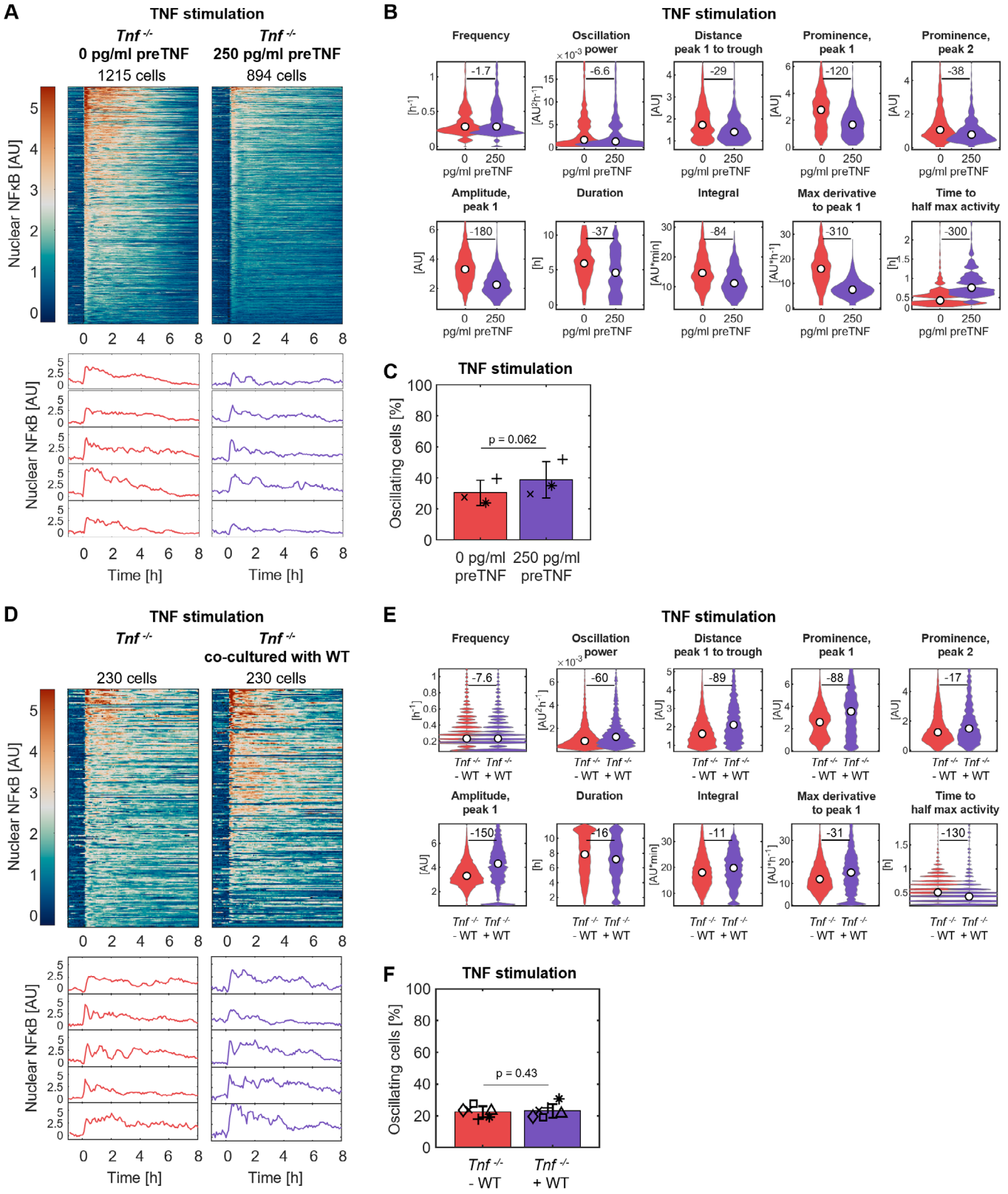

Figure EV1.

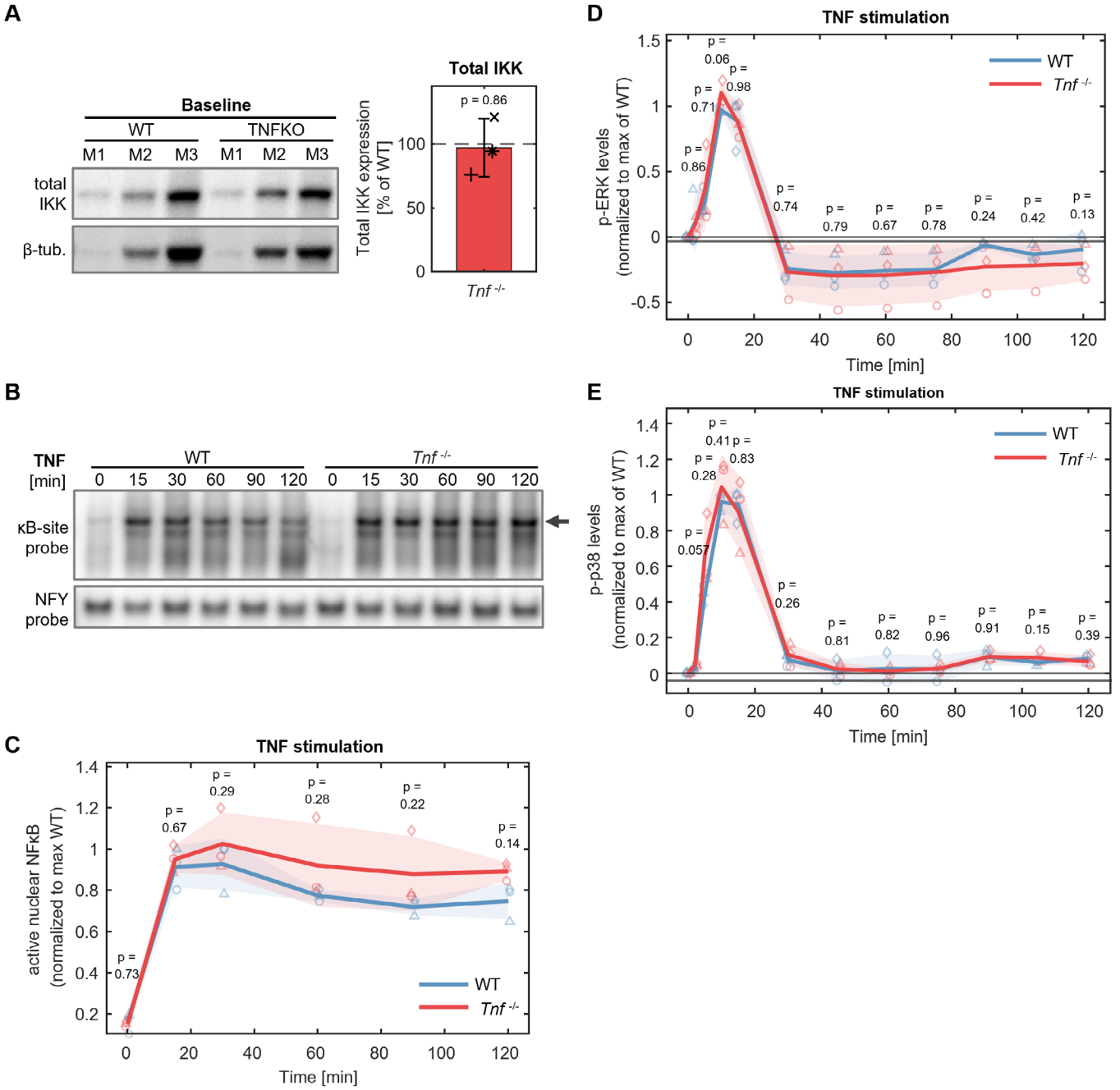

Figure EV2. Potential mechanisms controlling the oscillatory content in TNF-induced NFκB dynamics.

A Total IKK levels in unstimulated WT and *Tnf*$^{-/-}$ BMDMs, determined by SDS–PAGE followed by western blotting. (Left) Western Blot of total IKK and β-tubulin (β-tub.) of samples from three independent sets of BMDMs generation (M1-M3). (Right) For quantification, IKK levels in *Tnf*$^{-/-}$ cells were expressed as percentage of IKK levels in WT cells. Data are represented as mean ± SD of three biological replicates. Statistical significance was determined by two-tailed one-sample *t*-test using a hypothesis mean of 100.

B, C Levels of nuclear NFκB DNA-binding activity in WT and *Tnf*$^{-/-}$ BMDMs stimulated with 10 ng/ml TNF over 2 h, determined by EMSA. (B) One representative experiment is shown. The κB-site probe binds NFκB. The NF-Y probe serves as normalization control. (C) Quantification of the NFκB-DNA complex was normalized to the quantified NFY-DNA complex, and then to maximum WT value in each replicate. Data are represented as mean ± SD of three biological replicates. Statistical significance was determined by two-tailed paired-sample *t*-test for each time point. Data for *Tnf*$^{-/-}$ BMDMs are also shown in Fig 4E.

D, E Quantification of p-ERK p44 (D) and p-p38 (E) levels in WT and *Tnf*$^{-/-}$ BMDMs stimulated with 10 ng/ml TNF over 2 h, determined by western blotting as in Fig 2C. Basal levels (0 min) were deducted per genotype before normalizing to maximum WT value in each replicate. Data are represented as mean ± SD of three biological replicates. Statistical significance was determined by two-tailed paired-sample *t*-test for each time point.

Figure EV3. Mechanisms regulating TNF receptor turnover and signaling control oscillatory content in TNF-induced NFκB dynamics.

A, B Distribution of parameters and parameter combinations that can mediate less oscillatory responses used to simulate heterogeneous single-cell NFκB trajectories in "WT" and "*Tnf*$^{-/-}$" models in Fig 3B (A) or Fig EV3C (B). The "*Tnf*$^{-/-}$" population was modeled by shifting the mean of the parameter distributions by $10^{0.1}\times$ or $10^{-0.1}\times$.

C Simulated single-cell NFκB dynamics upon TNF stimulation over 8 h (heatmaps) in "WT" and "*Tnf*$^{-/-}$" models (row 1, row 2) as in Fig 3B. Results using parameters and parameter combinations that can mediate less oscillatory responses not shown in Fig 3B are shown here. Percentage of cells with oscillatory NFκB trajectories among all simulated responder cells (row 3) and oscillation power of simulated NFκB trajectories (row 4) are shown below. A total of 2,000 cells were simulated. Marker indicates median of distribution. Statistical significance was evaluated by Kolmogorov–Smirnov test. Number indicates $\log_{10}$(*P*-value).

D Simulated average IKK activity over 8 h in mathematical models of TNF-induced NFκB dynamics in "WT" and "*Tnf*$^{-/-}$" cells, as in (C).

E Simulated mean TNF receptor levels at steady state in mathematical models of TNF-induced NFκB dynamics in "WT" and "*Tnf*$^{-/-}$" cells, as in (C).

F TNF receptor 1 (TNFR1, left), TNF receptor 2 (TNFR2, center), and CD11b (right) cell surface expression in WT and *Tnf*$^{-/-}$ BMDMs unstimulated or stimulated for 30 min with 10 ng/ml TNF, measured by flow cytometry. Data are represented as mean ± SD of three culture replicates. One of three biological replicates is shown. Statistical significance was determined by unpaired two-tailed *t*-test. MFI, median fluorescence intensity.

G Nuclear localization of mVenus-RelA upon stimulation with 10 ng/ml TNF was measured over time by fluorescence microscopy in BMDMs of indicated genotypes pre-treated with TNFR1 siRNA, control (ctrl) siRNA, or untreated (–). Nuclear mVenus-RelA was quantified by automated image analysis. Each row of the heatmap represents the NFκB signaling trajectory of one cell. Trajectories are filtered for responding cells and sorted by maximum amplitude. Data from one of three biological replicates are depicted.

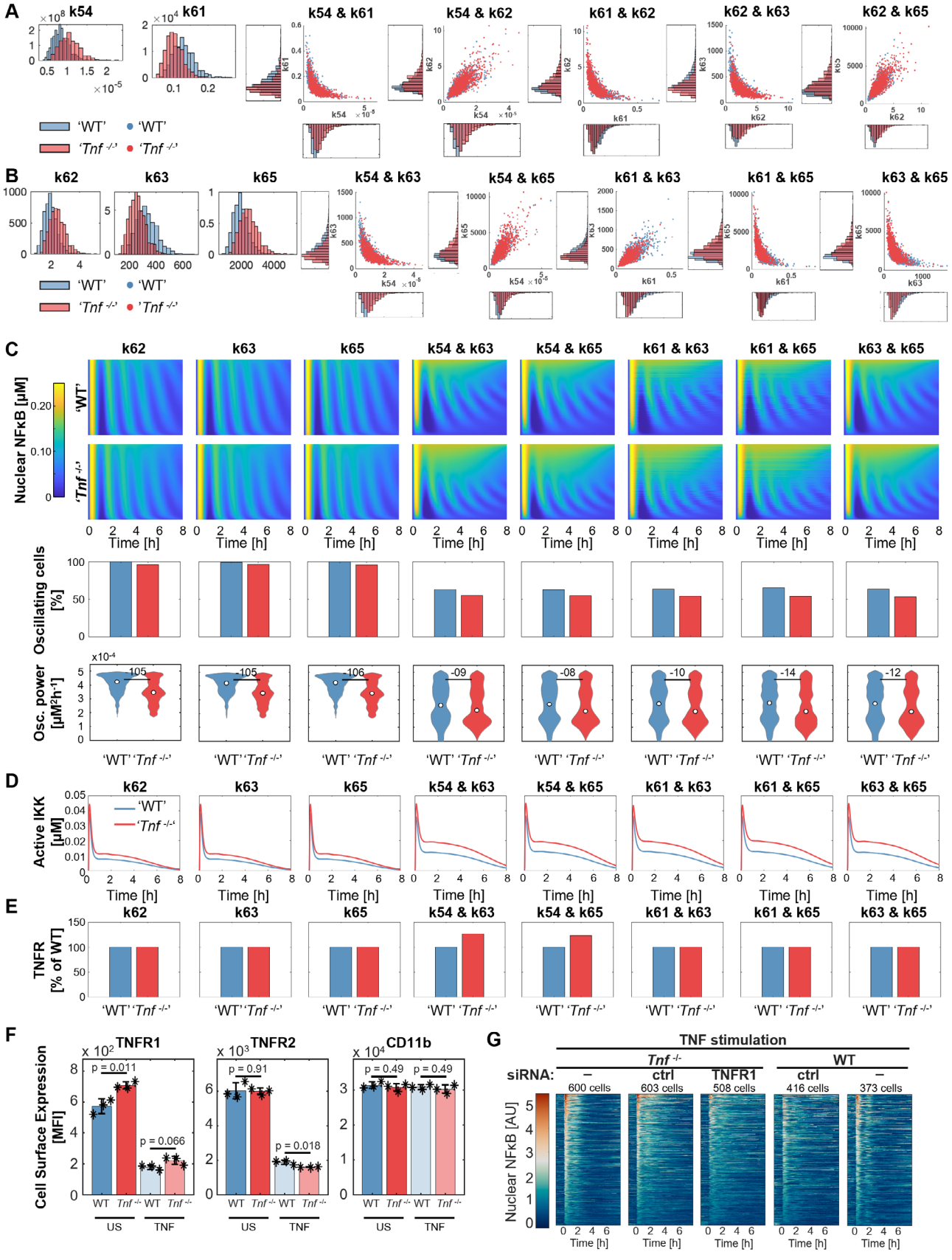

Figure EV3.

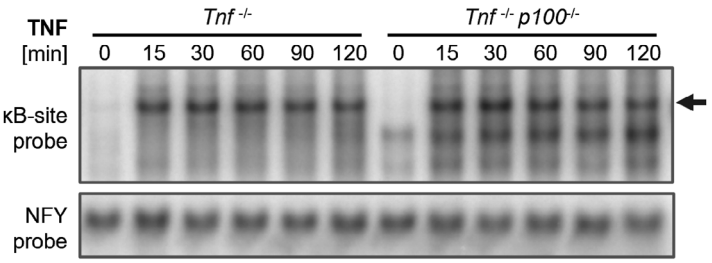

Figure EV4. NFκB EMSA in *Tnf* $^{-/-}$ BMDMs and *Tnf* $^{-/-}$p100$^{-/-}$ BMDMs.

Levels of nuclear NFκB DNA-binding activity in Tnf$^{-/-}$ and Tnf$^{-/-}$p100$^{-/-}$ BMDMs stimulated with 10 ng/ml TNF over 2 h, determined by EMSA. One representative experiment is shown. The κB-site probe binds NFκB. NFY probe serves as normalization control.

